# Integrated waveguide Bragg gratings for microwave photonics signal processing

**Maurizio Burla,**[1,*] **Luis Romero Cortés,**[1] **Ming Li,**[2] **Xu Wang,**[3] **Lukas Chrostowski,**[3] **and José Azaña**[1,4]

[1]*Institut National de la Recherche Scientifique – Énergie, Matériaux et Télécommunications (INRS-EMT) 1650 boulevard Lionel-Boulet, Varennes, QC, J3X 1S2, Canada*
[2]*Institute of Semiconductors, Chinese Academy of Sciences, No. 35, Tsinghua East Road, Beijing, 100083, China*
[3]*Department of Electrical and Computer Engineering, University of British Columbia, Vancouver, BC, V6T 1Z4, Canada*
[4]*azana@emt.inrs.ca*
[*]*maurizio.burla@gmail.com*

**Abstract:** Integrated Microwave photonics (IMWP) signal processing using Photonic Integrated Circuits (PICs) has attracted a great deal of attention in recent years as an enabling technology for a number of functionalities not attainable by purely microwave solutions. In this context, integrated waveguide Bragg grating (WBG) devices constitute a particularly attractive approach thanks to their compactness and flexibility in producing arbitrarily defined amplitude and phase responses, by directly acting on coupling coefficient and perturbations of the grating profile. In this article, we review recent advances in the field of integrated WBGs applied to MWP, analyzing the advantages leveraged by an integrated realization. We provide a perspective on the exciting possibilities offered by the silicon photonics platform in the field of MWP, potentially enabling integration of highly-complex active and passive functionalities with high yield on a single chip, with a particular focus on the use of WBGs as basic building blocks for linear filtering operations. We demonstrate the versatility of WBG-based devices by proposing and experimentally demonstrating a novel, continuously-tunable, integrated true-time-delay (TTD) line based on a very simple dual phase-shifted WBG (DPS-WBG).



**OCIS codes:** (060.5625) Radio frequency photonics; (070.1170) Analog optical signal processing; (130.3120) Integrated optics devices; (250.5300) Photonic integrated circuits; (130.6622) Subsystem integration and techniques; (070.7145) Ultrafast processing; (050.2770) Gratings; (060.3735) Fiber Bragg gratings.

## References and links

1. J. Capmany and D. Novak, "Microwave photonics combines two worlds," Nature Photon. **1**, 319–330 (2007).
2. A. J. Seeds and K. J. Williams, "Microwave photonics," J. Lightw. Technol. **24**, 4628–4641 (2006).
3. R. A. Minasian, "Photonic signal processing of microwave signals," IEEE Trans. Microw. Theory Tech. **54**, 832–846 (2006).
4. W. Ng, A. Walston, G. Tangonan, J. Lee, I. Newberg, and N. Bernstein, "The first demonstration of an optically steered microwave phased array antenna using true-time-delay," J. Lightw. Technol. **9**, 1124–1131 (1991).
5. D. Marpaung, C. Roeloffzen, R. Heideman, A. Leinse, S. Sales, and J. Capmany, "Integrated microwave photonics," Laser & Photon. Rev. **10.1002/lpor.201200032** (2013).
6. K. O. Hill, B. Malo, F. Bilodeau, D. C. Johnson, and J. Albert, "Bragg gratings fabricated in monomode photosensitive optical-fiber by UV exposure through a phase mask," Appl. Phys. Lett. **62**, 1035–1037 (1993).

#193416 - $15.00 USD Received 5 Jul 2013; revised 22 Sep 2013; accepted 27 Sep 2013; published 15 Oct 2013

7. R. Kashyap, *Fiber Bragg Gratings* (Academic Press, San Diego, 1999).
8. T. Erdogan, "Fiber grating spectra," J. Lightw. Technol. **15**, 1277–1294 (1997).
9. J. Skaar, L. Wang, and T. Erdogan, "On the synthesis of fiber Bragg gratings by layer peeling," IEEE J. Quantum Electron. **37**, 165–173 (2001).
10. M. Li and H. Li, "Reflection equalization of the simultaneous dispersion and dispersion-slope compensator based on a phase-only sampled fiber Bragg grating," Opt. Express **16**, 9821–9828 (2008).
11. M. Li, J. Hayashi, and H. Li, "Advanced design of a complex fiber Bragg grating for a multichannel asymmetrical triangular filter," J. Opt. Soc. Am. B **26**, 228–234 (2009).
12. B. Eggleton, B. Mikkelsen, G. Raybon, A. Ahuja, J. Rogers, P. Westbrook, T. Nielsen, S. Stulz, and K. Dreyer, "Tunable dispersion compensation in a 160-Gb/s TDM system by a voltage controlled chirped fiber Bragg grating," IEEE Photon. Technol. Lett. **12**, 1022–1024 (2000).
13. H. Li, M. Li, Y. Sheng, and J. Rothenberg, "Advances in the design and fabrication of high-channel-count fiber Bragg gratings," J. Lightw. Technol. **25**, 2739–2750 (2007).
14. L. Dong, P. Hua, T. Birks, L. Reekie, and P. Russell, "Novel add/drop filters for wavelength-division-multiplexing optical fiber systems using a Bragg grating assisted mismatched coupler," IEEE Photon. Technol. Lett., IEEE **8**, 1656–1658 (1996).
15. I. Baumann, J. Seifert, W. Nowak, and M. Sauer, "Compact all-fiber add-drop-multiplexer using fiber Bragg gratings," IEEE Photon. Technol. Lett. **8**, 1331–1333 (1996).
16. D. Pastor, J. Capmany, and B. Ortega, "Broad-band tunable microwave transversal notch filter based on tunable uniform fiber Bragg gratings as slicing filters," IEEE Photon. Technol. Lett. **13**, 726–728 (2001).
17. M. Li, H. Li, and Y. Painchaud, "Multi-channel notch filter based on a phase-shift phase-only sampled fiber Bragg grating," Opt. Express **16**, 19388–19394 (2008).
18. A. Galvanauskas, M. Fermann, D. Harter, K. Sugden, and I. Bennion, "All-fiber femtosecond pulse amplification circuit using chirped Bragg gratings," Appl. Phys. Lett. **66**, 1053–1055 (1995).
19. M. Rad, K. Fouli, H. Fathallah, L. Rusch, and M. Maier, "Passive optical network monitoring: challenges and requirements," IEEE Commun. Mag. **49**, s45–S52 (2011).
20. J. Hu, Z. Chen, X. Yang, J. Ng, and C. Yu, "100-km long distance fiber Bragg grating sensor system based on erbium-doped fiber and raman amplification," IEEE Photon. Technol. Lett. **22**, 1422–1424 (2010).
21. Y. Feng, L. R. Taylor, and D. B. Calia, "150 W highly-efficient raman fiber laser," Opt. Express **17**, 23678–23683 (2009).
22. Y.-J. Rao, "Recent progress in applications of in-fibre Bragg grating sensors," Opt. Laser Eng. **31**, 297–324 (1999).
23. Y. X. Luo, "Study of fiber Bragg grating sensor in dam safety monitoring," Applied Mechanics and Materials **312**, 736–740 (2013).
24. Y. Kim, S. Doucet, and S. LaRochelle, "50-channel 100-GHz-spaced multiwavelength fiber lasers with single-frequency and single-polarization operation," IEEE Photon. Technol. Lett. **20**, 1718–1720 (2008).
25. M. Li, X. Chen, T. Fujii, Y. Kudo, H. Li, and Y. Painchaud, "Multiwavelength fiber laser based on the utilization of a phase-shifted phase-only sampled fiber Bragg grating," Opt. Lett. **34**, 1717–1719 (2009).
26. M. Delgado-Pinar, D. Zalvidea, A. Diez, P. Perez-Millan, and M. Andres, "Q-switching of an all-fiber laser by acousto-optic modulation of a fiber Bragg grating," Opt. Express **14**, 1106–1112 (2006).
27. A. Molony, C. Edge, and I. Bennion, "Fibre grating time delay element for phased array antennas," Electron. Lett. **31**, 1485–1486 (1995).
28. H. Zmuda, R. A. Soref, P. Payson, S. Johns, and E. N. Toughlian, "Photonic beamformer for phased array antennas using a fiber grating prism," IEEE Photon. Technol. Lett. **9**, 241–243 (1997).
29. A. Molony, Z. Lin, J. A. R. Williams, I. Bennion, C. Edge, and J. Fells, "Fiber Bragg-grating true time-delay systems: discrete-grating array 3-b delay lines and chirped-grating 6-b delay lines," IEEE Trans. Microw. Theory Tech. **45**, 1527–1530 (1997).
30. Y. Liu, J. P. Yao, and J. Yang, "Wideband true-time-delay beam former that employs a tunable chirped fiber grating prism," Appl. Opt. **42**, 2273–2277 (2003).
31. J. L. Corral, J. Marti, J. M. Fuster, and R. I. Laming, "True time-delay scheme for feeding optically controlled phased-array antennas using chirped-fiber gratings," IEEE Photon. Technol. Lett. **9**, 1529–1531 (1997).
32. J. P. Yao, J. Yang, and Y. Liu, "Continuous true-time-delay beamforming employing a multiwavelength tunable fiber laser source," IEEE Photon. Technol. Lett. **14**, 687–689 (2002).
33. J. Capmany, B. Ortega, and D. Pastor, "A tutorial on microwave photonic filters," J. Lightw. Technol. **24**, 201–209 (2006).
34. D. Hunter and R. Minasian, "Reflectively tapped fibre optic transversal filter using in-fibre Bragg gratings," Electron. Lett. **31**, 1010–1012 (1995).
35. X. Yi and R. Minasian, "Dispersion induced RF distortion of spectrum-sliced microwave-photonic filters," IEEE Trans. Microw. Theory Tech. **54**, 880–886 (2006).
36. F. Zeng, J. Wang, and J. Yao, "All-optical microwave bandpass filter with negative coefficients based on a phase modulator and linearly chirped fiber Bragg gratings," Opt. Lett. **30**, 2203–2205 (2005).
37. G. H. Qi, J. P. Yao, J. Seregelyi, S. Paquet, and C. Belisle, "Generation and distribution of a wide-band con-

#193416 - $15.00 USD Received 5 Jul 2013; revised 22 Sep 2013; accepted 27 Sep 2013; published 15 Oct 2013

tinuously tunable millimeter-wave signal with an optical external modulation technique," IEEE Trans. Microw. Theory Tech. **53**, 3090–3097 (2005).
38. J. Liu, J. P. Yao, J. Yao, and T. H. Yeap, "Single-longitudinal-mode multiwavelength fiber ring laser," IEEE Photon. Technol. Lett. **14**, 1020–1022 (2004).
39. X. F. Chen, Z. C. Deng, and J. P. Yao, "Photonic generation of microwave signal using a dual-wavelength single-longitudinal-mode fiber ring laser," IEEE Trans. Microw. Theory Tech. **54**, 804–809 (2006).
40. J. Sun, Y. T. Dai, X. F. Chen, Y. J. Zhang, and S. Z. Xie, "Stable dual-wavelength DFB fiber laser with separate resonant cavities and its application in tunable microwave generation," IEEE Photon. Technol. Lett. **18**, 2587–2589 (2006).
41. Z. Li, C. Wang, M. Li, H. Chi, X. Zhang, and J. Yao, "Instantaneous microwave frequency measurement using a special fiber Bragg grating," IEEE Microw. Wireless Compon. Lett. **21**, 52–54 (2011).
42. J. Yao, "Photonic generation of microwave arbitrary waveforms," Optics Communications **284**, 3723 – 3736 (2011). Special Issue on Optical Pulse Shaping, Arbitrary Waveform Generation, and Pulse Characterization.
43. M. Abtahi, J. Magné, M. Mirshafiei, L. A. Rusch, and S. LaRochelle, "Generation of power-efficient FCC-compliant UWB waveforms using FBGs: Analysis and experiment," J. Lightw. Technol. **26**, 628–635 (2008).
44. J. A. na and L. R. Chen, "Synthesis of temporal optical waveforms by fiber Bragg gratings: a new approach based on space-to-frequency-to-time mapping," J. Opt. Soc. Am. B **19**, 2758–2769 (2002).
45. M. Li, L.-Y. Shao, J. Albert, and J. Yao, "Tilted fiber Bragg grating for chirped microwave waveform generation," IEEE Photon. Technol. Lett. **23**, 314–316 (2011).
46. M. Li, L.-Y. Shao, J. Albert, and J. Yao, "Continuously tunable photonic fractional temporal differentiator based on a tilted fiber Bragg grating," IEEE Photon. Technol. Lett. **23**, 251–253 (2011).
47. H. Shahoei, J. Yao *et al.*, "A continuously tunable multi-tap complex-coefficient microwave photonic filter based on a tilted fiber Bragg grating," Opt. Express **21**, 7521–7527 (2013).
48. R. Ashrafi, M. Li, N. Belhadj, M. Dastmalchi, S. LaRochelle, and J. Azaña, "Experimental demonstration of superluminal space-to-time mapping in long period gratings," Opt. Lett. **38**, 1419–1421 (2013).
49. R. Ashrafi, M. Li, and J. Azaña, "Tsymbol/s optical coding based on long-period gratings," IEEE Photon. Technol. Lett. **25**, 910–913 (2013).
50. R. Ashrafi, M. Li, and J. Azaña, "Coupling-strength-independent long-period grating designs for THz-bandwidth optical differentiators," Photonics Journal, IEEE **5**, 7100311–7100311 (2013).
51. R. Ashrafi, M. Li, S. LaRochelle, and J. Azaña, "Superluminal space-to-time mapping in grating-assisted co-directional couplers," Opt. Express **21**, 6249–6256 (2013).
52. R. Ashrafi and J. Azaña, "Terahertz bandwidth all-optical Hilbert transformers based on long-period gratings," Opt. Lett. **37**, 2604–2606 (2012).
53. T. E. Murphy, J. Ferrera, J. T. Hastings, M. J. Khan, E. M. Koontz, M. H. Lim, H. Haus, L. A. Kolodziejski, and H. I. Smith, "Development of fabrication techniques for building integrated-optical grating-based filters," [Online.] Available: http://nanoweb.mit.edu/annual-report00/16 .
54. T. Berceli and P. Herczfeld, "Microwave photonics - a historical perspective," IEEE Trans. Microw. Theory Tech. **58**, 2992–3000 (2010).
55. R. Won, "Microwave photonics shines," Nature Photon. **5**, 736 (2011).
56. J. Capmany, J. Mora, I. Gasulla, J. Sancho, J. Lloret, and S. Sales, "Microwave photonic signal processing," J. Lightw. Technol. **31**, 571–586 (2013).
57. S. T. Chu, B. E. Little, J. V. Hryniewicz, F. G. Johnson, O. King, D. Gill, W. Chen, and W. Chen, "High Index Contrast Photonics Platform," in "Proc. of SPIE," vol. 6014, A. K. Dutta, Y. Ohishi, N. K. Dutta, and J. Moerk, eds. (2005), vol. 6014, pp. 1–10.
58. G. Roelkens, L. Liu, D. Liang, R. Jones, A. Fang, B. Koch, and J. Bowers, "III-V/silicon photonics for on-chip and intra-chip optical interconnects," Laser & Photon. Rev. **4**, 751–779 (2010).
59. M. Davenport, J. Bauters, M. Piels, A. Chen, A. Fang, and J. E. Bowers, "A 400 Gb/s WDM receiver using a low loss silicon nitride AWG integrated with hybrid silicon photodetectors," in "Optical Fiber Communication Conference/National Fiber Optic Engineers Conference 2013," (Optical Society of America, 2013), p. PDP5C.5.
60. T.-Y. Liow, J. Song, X. Tu, A.-J. Lim, Q. Fang, N. Duan, M. Yu, and G.-Q. Lo, "Silicon optical interconnect device technologies for 40 Gb/s and beyond," IEEE J. Sel. Topics Quantum Electron. **19**, 8200312–8200312 (2013).
61. J. F. Bauters, M. J. R. Heck, D. D. John, J. S. Barton, C. M. Bruinink, A. Leinse, R. G. Heideman, D. J. Blumenthal, and J. E. Bowers, "Planar waveguides with less than 0.1 dB/m propagation loss fabricated with wafer bonding," Opt. Express **19**, 24090–24101 (2011).
62. B. R. Koch, E. J. Norberg, B. Kim, J. Hutchinson, J.-H. Shin, G. Fish, and A. Fang, "Integrated silicon photonic laser sources for telecom and datacom," in "Optical Fiber Communication Conference/National Fiber Optic Engineers Conference 2013," (Optical Society of America, 2013), p. PDP5C.8.
63. M. Hochberg, N. Harris, R. Ding, Y. Zhang, A. Novack, Z. Xuan, and T. Baehr-Jones, "Silicon photonics: the next fabless semiconductor industry," IEEE Solid-State Circuits Magazine **5**, 48–58 (2013).
64. T. Baehr-Jones, R. Ding, A. Ayazi, T. Pinguet, M. Streshinsky, N. Harris, J. Li, L. He, M. Gould, Y. Zhang, A. E.-J. Lim, T.-Y. Liow, S. H.-G. Teo, G.-Q. Lo, and M. Hochberg, "A 25 Gb/s silicon photonics platform,"

#193416 - $15.00 USD Received 5 Jul 2013; revised 22 Sep 2013; accepted 27 Sep 2013; published 15 Oct 2013

arXiv:1203.0767 (2012).
65. M. Strain and M. Sorel, "Design and fabrication of integrated chirped Bragg gratings for on-chip dispersion control," IEEE J. Quantum Electron. **46**, 774–782 (2010).
66. X. Wang, W. Shi, H. Yun, S. Grist, N. A. F. Jaeger, and L. Chrostowski, "Narrow-band waveguide Bragg gratings on SOI wafers with CMOS-compatible fabrication process," Opt. Express **20**, 15547–15558 (2012).
67. M. Verbist, D. V. Thourhout, and W. Bogaerts, "Weak gratings in silicon-on-insulator for spectral filters based on volume holography," Opt. Lett. **38**, 386–388 (2013).
68. A. D. Simard, Y. Painchaud, and S. LaRochelle, "Integrated Bragg gratings in spiral waveguides," Opt. Express **21**, 8953–8963 (2013).
69. W. Li, M. Li, and J. Yao, "A narrow-passband and frequency-tunable microwave photonic filter based on phase-modulation to intensity-modulation conversion using a phase-shifted fiber Bragg grating," IEEE Trans. Microw. Theory Tech. **60**, 1287–1296 (2012).
70. D. Marpaung, C. Roeloffzen, A. Leinse, and M. Hoekman, "A photonic chip based frequency discriminator for a high performance microwave photonic link," Opt. Express **18**, 27359–27370 (2010).
71. B. Zhou, X. Zheng, X. Yu, H. Zhang, Y. Guo, and B. Zhou, "Impact of group delay ripples of chirped fiber grating on optical beamforming networks," Opt. Express **16**, 2398–2404 (2008).
72. T. Niemi, M. Uusimaa, and H. Ludvigsen, "Limitations of phase-shift method in measuring dense group delay ripple of fiber Bragg gratings," IEEE Photon. Technol. Lett. **13**, 1334–1336 (2001).
73. M. Sumetsky, B. Eggleton, and C. de Sterke, "Theory of group delay ripple generated by chirped fiber gratings," Opt. Express **10**, 332–340 (2002).
74. X. Liu, L. Mollenauer, and X. Wei, "Impact of group-delay ripple in transmission systems including phase-modulated formats," IEEE Photon. Technol. Lett. **16**, 305–307 (2004).
75. M. A. Schneider and S. Mookherjea, "Modeling light transmission in silicon waveguides," in Conference on Lasers and Electro-Optics 2012, OSA Technical Digest (online) (Optical Society of America, 2012), paper CM4A.1.
76. L. He, Y. Liu, C. Galland, A. E. J. Lim, G. Q. Lo, T. Baehr-Jones, and M. Hochberg, "A High-Efficiency Nonuniform Grating Coupler Realized With 248-nm Optical Lithography," IEEE Photon. Technol. Lett., **25**, 1358–1361 (2013).
77. N. Na, H. Frish, I-Wei Hsieh, O. Harel, R. George, A. Barkai, and H. Rong, "Efficient broadband silicon-on-insulator grating coupler with low backreflection," Opt. Lett. **36**, 2101–2103 (2011)
78. S. Khan and S. Fathpour, "Electronically tunable silicon photonic delay lines," in "2010 23rd Annual Meeting of the IEEE Photonics Society," (2010), pp. 234–235.
79. I. Giuntoni, D. Stolarek, D. I. Kroushkov, J. Bruns, L. Zimmermann, B. Tillack, and K. Petermann, "Continuously tunable delay line based on SOI tapered Bragg gratings," Opt. Express **20**, 11241–11246 (2012).
80. X. Wang, H. Yun, and L. Chrostowski, "Integrated Bragg gratings in spiral waveguides," in "CLEO: 2013," (Optical Society of America, 2013), p. CTh4F.8.
81. K. Rutkowska, D. Duchesne, M. Strain, R. Morandotti, M. Sorel, and J. Azaña, "Ultrafast all-optical temporal differentiators based on CMOS-compatible integrated-waveguide Bragg gratings," Opt. Express **19**, 19514–19522 (2011).
82. M. Ferrera, Y. Park, L. Razzari, B. E. Little, S. T. Chu, R. Morandotti, D. J. Moss, and J. Azaña, "On-chip CMOS-compatible all-optical integrator," Nat. Commun. **1** (2010).
83. M. J. Khan, *Integrated Optical Filters using Bragg Gratings and Resonators* (Ph.D. thesis, Massachussets Institute of Technology, 2002).
84. M. Strain, *Integrated Chirped Bragg Gratings for Dispersion Control* (Ph.D. thesis, University of Glasgow, 2007), http://theses.gla.ac.uk/440/.
85. M. G. Wickham, "Integrated optical time delay unit," United States Patent (1997).
86. M. Rasras, C. Madsen, M. Cappuzzo, E. Chen, L. Gomez, E. Laskowski, A. Griffin, A. Wong-Foy, A. Gasparyan, A. Kasper, J. Grange, and S. Patel, "Integrated resonance-enhanced variable optical delay lines," IEEE Photon. Technol. Lett. **17**, 834–836 (2005).
87. F. Xia, L. Sekaric, and Y. Vlasov, "Ultracompact optical buffers on a silicon chip," Nature Photon. **1**, 65–71 (2007).
88. A. Yariv, Y. Xu, R. K. Lee, and A. Scherer, "Coupled-resonator optical waveguide: a proposal and analysis," Opt. Lett. **24**, 711–713 (1999).
89. M. Spasojevic and L. R. Chen, "Discretely tunable optical delay lines using serial and step-chirped sidewall Bragg gratings in SOI," Electron. Lett. **49** (2013).
90. M. Spasojevic and L. R. Chen, "Tunable optical delay line in SOI implemented with step chirped Bragg gratings and serial grating arrays," in "Photonics North," (2013).
91. S. T. Abraha, C. M. Okonkwo, E. Tangdiongga, and A. M. J. Koonen, "Power-efficient impulse radio ultrawideband pulse generator based on the linear sum of modified doublet pulses," Opt. Lett. **36**, 2363–2365 (2011).
92. D. Marpaung, L. Chevalier, M. Burla, and C. Roeloffzen, "Impulse radio ultrawideband pulse shaper based on a programmable photonic chip frequency discriminator," Opt. Express **19**, 24838–24848 (2011).
93. J. Azaña, "Ultrafast analog all-optical signal processors based on fiber-grating devices," Photonics Journal, IEEE

#193416 - $15.00 USD Received 5 Jul 2013; revised 22 Sep 2013; accepted 27 Sep 2013; published 15 Oct 2013

**2**, 359–386 (2010).
94. M. A. Preciado and M. A. Muriel, "Design of an ultrafast all-optical differentiator based on a fiber Bragg grating in transmission," Opt. Lett. **33**, 2458–2460 (2008).
95. L. Rivas, K. Singh, A. Carballar, and J. Azaña, "Arbitrary-order ultrabroadband all-optical differentiators based on fiber Bragg gratings," IEEE Photon. Technol. Lett. **19**, 1209–1211 (2007).
96. M. Li, D. Janner, J. Yao, and V. Pruneri, "Arbitrary-order all-fiber temporal differentiator based on a fiber Bragg grating: design and experimental demonstration," Opt. Express **17**, 19798–19807 (2009).
97. M. Kulishov and J. Azaña, "Design of high-order all-optical temporal differentiators based on multiple-phase-shifted fiber Bragg gratings," Opt. Express **15**, 6152–6166 (2007).
98. C. Sima, J. C. Gates, H. L. Rogers, P. L. Mennea, C. Holmes, M. N. Zervas, and P. G. R. Smith, "Phase controlled integrated interferometric single-sideband filter based on planar Bragg gratings implementing photonic Hilbert transform," Opt. Lett. **38**, 727–729 (2013).
99. M. Li and J. Yao, "All-fiber temporal photonic fractional Hilbert transformer based on a directly designed fiber Bragg grating," Opt. Lett. **35**, 223–225 (2010).
100. M. Li and J. Yao, "Experimental demonstration of a wideband photonic temporal Hilbert transformer based on a single fiber Bragg grating," IEEE Photon. Technol. Lett. **22**, 1559–1561 (2010).
101. M. H. Asghari and J. Azaña, "All-optical Hilbert transformer based on a single phase-shifted fiber Bragg grating: design and analysis," Opt. Lett. **34**, 334–336 (2009).
102. C. Sima, J. C. Gates, C. Holmes, P. L. Mennea, M. N. Zervas, and P. G. R. Smith, "Terahertz bandwidth photonic Hilbert transformers based on synthesized planar Bragg grating fabrication," Opt. Lett., **38**, 3448–3451 (2013).
103. J. Ge, C. Wang, and X. Zhu, "Fractional optical Hilbert transform using phase shifted fiber Bragg gratings," Opt. Commun. **284**, 3251 – 3257 (2011).
104. C. Sima, J. Gates, H. Rogers, C. Holmes, M. Zervas, and P. Smith, "Integrated all-optical ssb modulator using photonic Hilbert transformer with planar Bragg gratings," in "CLEO/Europe and EQEC 2011 Conference Digest," (Optical Society of America, 2011), pp. CI4–5.
105. E. H. Bernhardi, M. R. H. Khan, C. G. H. Roeloffzen, H. A. G. M. van Wolferen, K. Wörhoff, R. M. de Ridder, and M. Pollnau, "Photonic generation of stable microwave signals from a dual-wavelength $Al_2O_3$:$Yb^{3+}$ distributed-feedback waveguide laser," Opt. Lett. **37**, 181–183 (2012).
106. M. R. H. Khan, E. Bernhardi, D. A. I. Marpaung, M. Burla, R. De Ridder, K. Worhoff, M. Pollnau, and C. G. H. Roeloffzen, "Dual-frequency distributed feedback laser with optical frequency locked loop for stable microwave signal generation," IEEE Photon. Technol. Lett. **24**, 1431–1433 (2012).
107. X. Wang, H. Yun, N. A. F. Jaeger, and L. Chrostowski, "Multi-Period Bragg Gratings in Silicon Waveguides", in "IEEE International Photonics Conference 2013 (IPC 2013)", accepted for publication.
108. R. J. Mailloux, *Phased Array Antenna Handbook* (Artech House, Boston, MA, 2005).
109. J. Yao, "Microwave photonics," J. Lightw. Technol. **27**, 314–335 (2009).
110. X. Wang, J. Flueckiger, S. Schmidt, S. Grist, S. T. Fard, J. Kirk, M. Doerfler, K. C. Cheung, D. M. Ratner, and L. Chrostowski, "A silicon photonic biosensor using phase-shifted Bragg gratings in slot waveguide," J. Biophotonics (2013).
111. M. Burla, D. Marpaung, L. Zhuang, C. Roeloffzen, M. R. Khan, A. Leinse, M. Hoekman, and R. Heideman, "On-chip CMOS compatible reconfigurable optical delay line with separate carrier tuning for microwave photonic signal processing," Opt. Express **19**, 21475–21484 (2011).
112. A. Loayssa and F. Lahoz, "Broad-band RF photonic phase shifter based on stimulated Brillouin scattering and single-sideband modulation," IEEE Photon. Technol. Lett. **18**, 208–210 (2006).
113. M. Burla, D. Marpaung, L. Zhuang, A. Leinse, M. Hoekman, R. Heideman, C. Roeloffzen, "Integrated Photonic $K_u$-Band Beamformer Chip with Continuous Amplitude and Delay Control," IEEE Photon. Technol. Lett., **25**, 1145-1148 (2013).
114. M. Burla, C. G. Roeloffzen, L. Zhuang, D. Marpaung, M. R. Khan, P. Maat, K. Dijkstra, A. Leinse, M. Hoekman, and R. Heideman, "System integration and radiation pattern measurements of a phased array antenna employing an integrated photonic beamformer for radio astronomy applications," Appl. Opt., **51**, 789–802 (2012).
115. L. Zhuang, D. Marpaung, M. Burla, W. Beeker, A. Leinse, and C. Roeloffzen, "Low-loss, high-index-contrast $Si_3N_4$/$SiO_2$ optical waveguides for optical delay lines in microwave photonics signal processing," Opt. Express, **19**, 23162–23170 (2011).
116. X. Wang, W. Shi, S. Grist, H. Yun, N. Jaeger, and L. Chrostowski, "Narrow-band transmission filter using phase-shifted Bragg gratings in SOI waveguide," in 2011 IEEE Photonics Conference, (2011), pp. 869–870.
117. W. Shi, X. Wang, W. Zhang, L. Chrostowski, and N. A. F. Jaeger, "Contradirectional couplers in silicon-on-insulator rib waveguides," Opt. Lett. **36**, 3999–4001 (2011).
118. W. Shi, X. Wang, C. Lin, H. Yun, Y. Liu, T. Baehr-Jones, M. Hochberg, N. A. F. Jaeger, and L. Chrostowski, "Silicon photonic grating-assisted, contra-directional couplers," Opt. Express **21**, 3633–3650 (2013).
119. D. Tan, K. Ikeda, S. Zamek, A. Mizrahi, M. Nezhad, A. Krishnamoorthy, K. Raj, J. Cunningham, X. Zheng, I. Shubin, Y. Luo, and Y. Fainman, "Wide bandwidth, low loss 1 by 4 wavelength division multiplexer on silicon for optical interconnects," Opt. Express **19**, 2401–2409 (2011).
120. W. Shi, H. Yun, C. Lin, M. Greenberg, X. Wang, Y. Wang, S. T. Fard, J. Flueckiger, N. A. F. Jaeger, and L. Chros-

#193416 - $15.00 USD Received 5 Jul 2013; revised 22 Sep 2013; accepted 27 Sep 2013; published 15 Oct 2013

towski, "Ultra-compact, flat-top demultiplexer using anti-reflection contra-directional couplers for CWDM networks on silicon," Opt. Express **21**, 6733–6738 (2013).
121. M. H. Khan, H. Shen, Y. Xuan, L. Zhao, S. Xiao, D. E. Leaird, A. M. Weiner, and M. Qi, "Ultrabroad-bandwidth arbitrary radiofrequency waveform generation with a silicon photonic chip-based spectral shaper," Nat Photon **4**, 117–122 (2010).
122. J. Capmany, S. Sales, I. Gasulla, J. Mora, J. Lloret, and J. Sancho, "Innovative concepts in microwave photonics," Waves [Online.] Available: http://www.iteam.upv.es/revista/2012/5_ITEAM_2012.pdf (2012).
123. I. Gasulla and J. Capmany, "Analog filtered links: A unifying approach for microwave photonic systems," in "14th International Conference on Transparent Optical Networks (ICTON)," (2012), pp. 1–4.

## 1. Introduction

The large amount of work done in the field of microwave photonics (MWP) [1–3] has shown that the use of optical technology can provide unprecedented performance and novel functionalities to the generation, transport, and processing of radio waves with frequencies up to the THz range. The initial development of MWP originated mainly from the need to transport high frequency signals over large distances, in particular to feed large antenna arrays. The main driving force for the introduction of photonics solutions in microwave engineering has been the extremely low-loss, low-cost and ultra-broadband performance of optical fibers when compared to any other type of transmission media for high-frequency electronic signals. Initially, the development of MWP solutions was carried on within the military research framework, for very high performance systems (e.g. wideband radar applications, antenna remoting and control using optical fibers in very large radar antennas) [4]. Over the years, with the cost reduction of commercial photonic components, MWP solutions started to spread towards a variety of applications, and the current growing demand for gigabit/s broadband wireless access networks is considered as one of the main drivers for the future diffusion of MWP [5] to the field of personal communications. Current application fields of MWP include optical control of antenna arrays, microwave filtering, generation of high-purity microwave signal or arbitrary waveforms, instantaneous frequency measurement of high-frequency signals, radio-over-fiber and photonic analog-to-digital conversion. A very large number of advances in many of these applications has been based on the use of a specific type of photonic device, namely the fiber Bragg grating (FBG). The possibility of implementing these fiber devices in integrated platforms (on-chip), so-called waveguide Bragg gratings (WBGs), has attracted considerable recent attention, with several demonstrated applications in the MWP context, as will be reviewed in Section 4 of this paper. This prospect is especially promising to overcome the intrinsic limitations (high cost, bulkiness, high power consumption etc.) of MWP devices and systems based on discrete components (e.g. FBGs) by realization of entire functionalities on a chip, a field that is usually referred to as integrated MWP (IMWP) [5]. This paper presents a detailed overview of progress to date on the use of WBGs for MWP applications. Additionally, to illustrate further the potential of this approach, in this work we present a novel and particularly simple approach to the implementation of optically-assisted microwave delay unit based on a very simple, uniform and non-apodized integrated dual phase-shifted WBG.

The paper is structured as follows. In Section 2 we give a brief overview on the use of FBGs in MWP applications. Section 3 introduces the field of IMWP and describes advantages and current challenges of the integrated implementation of Bragg gratings. Section 4 aims at providing a brief review of MWP solutions featuring WBGs as core signal processing units. In particular, in Section 5 we propose and demonstrate a novel integrated true-time-delay (TTD) line based on a very simple dual phase-shifted WBG. Finally, Section 7 presents a perspective on the potential of integrated WBGs in silicon as basic signal processing units for the implementation of complex MWP functionalities.

#193416 - $15.00 USD Received 5 Jul 2013; revised 22 Sep 2013; accepted 27 Sep 2013; published 15 Oct 2013

## 2. Fiber Bragg gratings in microwave photonics

A fiber Bragg grating (FBG) is a (quasi-)periodic perturbation of the effective refractive index along the length of an optical fiber. This is realized by exposure to an intense optical interference pattern, exploiting the photosensitivity of specific fiber materials [6, 7]. The resulting periodic structure in the optical fiber essentially acts as a wavelength-selective mirror. Depending on the average effective refractive index $n_{\text{eff}}$ and the grating period $\Lambda$, part of an incident wave is coupled to a counter-propagating mode in a strongly wavelength-selective manner, thus creating a stopband in the FBG transmission response, and a corresponding passband in the reflection response.

Well-proved design tools, essentially based on coupled-mode theory [8], are readily available to design the grating profile of an FBG (typically, the grating period variation and coupling strength along the device length) so that to achieve almost any desired complex (amplitude and phase) spectral transfer function in the FBG reflection response. Particularly, weak-coupling FBGs can be easily designed using the direct Fourier transform relationship between the grating local complex coupling coefficient (as a function of the grating length) and its reflection spectral response [9, 10]. For stronger gratings, more general inverse scattering algorithms, e.g. so-called layer-peeling methods, have been also developed and extensively tested [9, 11]. This unique design versatility, combined with the maturity of present fiber grating fabrication technologies, have led to the extensive use of FBG in a very large number of applications, mainly in the fiber-optics telecommunication world, including dispersion compensation [10, 12, 13], wavelength add/drop filters for optical communications [14, 15], notch filters [16, 17], fiber amplifiers [18], network monitoring [19], Raman amplification [20,21], distributed sensing [22,23] and fiber lasers [24–26]. The wide success of FBGs in such a variety of applications can be also understood by considering their numerous advantages, which are intrinsic to their all-fiber geometry. FBG devices are simple, relatively low cost, have very low losses, and provide full compatibility with fiber optic devices and systems.

MWP applications have exploited these same advantageous features of FBGs for radio-frequency (RF) signal generation, processing, and measurement. For example, FBGs with different central frequencies can be placed at different distances along a single fiber to create wavelength-selective reflectors used to implement a switched optical delay line. This has been extensively used for example for optical control of antenna arrays [27]. Often the delay lines realized in this manner have been grouped to form so-called fiber grating prisms, where a single laser source controls multiple fiber delays, each connected to a single antenna element [28, 29]. Chirped fiber Bragg gratings (CFBGs) have also been employed for the same purpose in order to achieve continuously tunable delay values [30–32]. A large number of works exploit delay lines based on both FBGs and CFBGs for implementation of incoherent multitap microwave photonic filters (MPF) [33–36]. Several authors have suggested the use of FBGs for microwave signal generation [37–40] and, more recently, for instantaneous frequency measurements [41]. A number of works have also demonstrated the use of FBGs for broadband arbitrary waveform generation [42–44].

Tilted FBGs have also been employed for microwave photonics applications, for example in arbitrary waveform generation, pulse shaping and microwave photonic filtering [45–47]. Very recently, long period gratings have been proposed as an alternative to fiber Bragg gratings to achieve larger processing bandwidth, which for FBGs is limited to a value in the order of 100 GHz. Several works have been recently proposed [48–52]. Those devices could be foreseen as potentially promising for MWP signal processing in the future.

#193416 - $15.00 USD Received 5 Jul 2013; revised 22 Sep 2013; accepted 27 Sep 2013; published 15 Oct 2013

## 3. Integrated waveguide Bragg gratings

### *3.1. Integrated microwave photonics*

To enable the envisioned spread of MWP solutions into commercial applications and in the telecommunication market, it is necessary to develop low-cost devices that can be manufactured on a large scale, that are compact and can be integrated with electronics and other optical components [53]. In fact, despite the promising results of the mentioned proof-of-principle demonstrations, several factors still preclude the practical use of many of the proposed MWP solutions. Photonics solutions proposed over the years have shown the desired high performance in terms of ultra-broad bandwidth and exceptional reconfigurability. However, they are often regarded with certain skepticism by the microwave engineering communities due to the generally low dynamic range and significant cost. These drawbacks can be mainly attributed to the fact that many MWP solutions are based on bulk optics and/or discrete standard optoelectronic devices. Notice that solutions based on free-space optics are additionally bulky and relatively unreliable for practical uses [5]. In this context, it is widely accepted [5, 54–56] that the emerging field of integrated microwave photonics (IMWP) can provide the answer to this need, i.e. as an enabling technology to exploit the unique performance advantages of MWP while leading to the large-scale deployment that is necessary in commercial applications. In fact, in addition to the well-known advantages of photonics, integrated solutions also offer compactness, light weight, and low power consumption. Moreover, these solutions promise to reduce the per-unit cost thanks to the high yield and reproducibility when realized with CMOS compatible fabrication equipment [57].

Particularly attractive is the availability of integrated active components such as modulators and photodetectors (PDs) in indium phosphide (InP) III/V technology or in silicon, which enables the potential realization of entire complex MWP systems on a chip [58–60].

The main drive behind the recent progress in integration has been the rapidly-increasing need for bandwidth in optical telecommunications and in high-density interconnections within data centers. In view of the current data-rate growth speed, the only viable way to increase the data handling speed without prohibitively increasing cost, size and power consumption appears the migration from the use of discrete components towards integrated systems [59]. MWP shares the same need for photonic integration and, as such, it can take advantage of this trend in telecom and datacom systems. Recent demonstrations have shown very successful results in this direction, showing the integration of silicon nitride waveguides featuring ultra-low loss [61] with a silicon layer and InGaAs photodetector arrays. A functional WDM receiver with 8 PDs with a 3 dB bandwidth of 30 GHz has been recently demonstrated [59], as well as silicon photonic laser array sources with performance approaching the one of native substrate lasers [62]. Those lasers employ an efficient III/V gain medium whereas silicon is used to define the laser cavity; light is efficiently transferred between the two media using mode couplers. Both laser types can be processed simultaneously on the same wafer, employing a commercial foundry, in the framework of a multi-project wafer approach.

Moreover, the system performance of active components and non-reciprocal devices (optical isolators and circulators) realized directly in silicon is quickly improving and, with the exception of laser sources, all the key functionalities can be implemented at a reasonably competitive performance level [63]. Recently, a 25 Gb/s photonics platform has been demonstrated [64], with parameters that approach towards the stringent system requirements of analog signal processing applications of MWP. The described platform is highly-accessible to the system design community thanks to a photonic shuttle service via multi-project wafer runs. The main strength of silicon photonics compared to other technologies is the ability to reach extremely high yields, with hundreds of thousands of working devices on a single wafer, thanks to the fact that they use exactly the same production facilities and tools of modern CMOS foundries.

#193416 - $15.00 USD Received 5 Jul 2013; revised 22 Sep 2013; accepted 27 Sep 2013; published 15 Oct 2013

### 3.2. *Integrated WBGs: advantages and challenges*

One of the main motivations of using Bragg grating devices for microwave and optical signal processing is their flexibility: the linear spectral transfer function, or corresponding temporal impulse response, of a Bragg grating device can be arbitrarily designed using many readily available design and synthesis methods [9, 11, 44] and subsequently fabricated with high tolerance. As detailed above, this design flexibility has enabled the realization of many fundamental functionalities for MWP applications and beyond. A natural way to translate these functionalities on a chip appears to be the use of integrated WBGs. Those components promise to retain the high level of flexibility reached with FBG designs, plus bringing specific advantages owing to the integrated realization. Notice that WBGs can be designed using a similar set of analysis and synthesis tools as FBGs [65]. Recent developments have enabled fabrication of WBGs with complex grating profiles [66–68].

Moreover, as anticipated, the use of WBGs brings additional specific advantages due to the integrated realization. Fiber gratings employ direct refractive index variations obtained in most cases by a photosensitive process. The index perturbation that can be achieved in this way is typically limited to $\pm 10^{-3}$ resulting in coupling coefficients in the order of 10 $cm^{-1}$ [65].

The realization of gratings in integrated form, instead, relies on the physical corrugation or perturbation of the waveguide geometry and on the depth of the etching process. This translates into a two-fold advantage, that is, (i) fabrication does not rely upon a photosensitive process, thus a wider variety of materials can be used; and (ii) this allows the realization of much higher grating coupling strengths (coupling coefficients exceeding 1,200 $cm^{-1}$ have been reported [81]) which, in turn, enables the implementation of devices that are significantly more compact than their fiber-optics counterparts, i.e. devices can be made very broadband (with operational bandwidths well into the THz range) while retaining a short length (up to a few millimeters).

Hence, in place or together with optical ring resonators (ORR), WBGs could effectively be used as basic signal processing blocks, thanks to their high design and operation flexibility, with the additional and fundamental advantage of operating in single-mode, thus offering a free-spectral range (FSR) not limited by the physical minimum waveguide bending radius as in the case of RRs. This later constraint represents the practical upper limit to the device bandwidth in most applications of RRs [82]. As mentioned above, WBG-based processors with instantaneous bandwidths well into the THz-range have been demonstrated [81].

All the mentioned advantages of WBGs come without compromising the design flexibility. The fact that the geometries are defined by fabrication processes that do not rely on complex interferometric processes allows a higher control in designing the properties of integrated Bragg grating structures [83].

Furthermore, a planar fabrication process allows a finer control over the grating dimensions, for example one can readily achieve sharp grating strength variations, and a very precise period control, including well-defined phase shifts along the grating [53].

Finally, on-chip Bragg gratings can be readily integrated with other well-defined waveguide components and building blocks, such as directional couplers, Y-junctions, waveguide bends, resonators, and more, allowing to implement complex filters and layouts [53]. The separation of input, transmission and reflection ports can be realized on-chip without the need of bulky and expensive isolators and circulators [83] (see also further discussions in Section 6 below on a recent contra-directional coupler configuration for optimized retrieval of the reflective response of Bragg gratings). When implemented on materials that support active functionalities, gratings can be integrated with tunable elements that allow reconfigurability of operation at a much faster speed and in a more energetically efficient fashion than with (most widely used) temperature control. As discussed above, especially interesting for MWP is the fact that modulators, detectors and phase shifters could be integrated on the same chip, potentially allowing to

#193416 - $15.00 USD Received 5 Jul 2013; revised 22 Sep 2013; accepted 27 Sep 2013; published 15 Oct 2013

realize complete MWP systems, including active and passive functionalities, on the same platform. In particular, when realizing gratings in silicon photonics, the possibility to use CMOS compatible fabrication equipment allows the realization of a large number of devices in a single wafer, similarly to the approach used in microelectronics, with benefits in terms of uniformity and low cost compared to fiber devices.

A number of challenges still remain. As the size of the integrated grating structures is generally much smaller than on fibers (Fig. 1), the waveguide non-uniformity (roughness) becomes relatively more significant, typically resulting in stronger ripples in their optical spectral responses. This is expected to have a particularly strong effect on all applications that require high passband uniformity, e.g. signal-processing operations based on phase modulation to intensity modulation conversion [69, 70]. Another related limitation involves the group delay ripples created by interference effects due to imperfections in the realization of the grating [71, 72]. These ripples represent a main drawback for time-delay applications of fiber or integrated-WBGs. Several studies have analyzed this problem in detail and studied its impact at the system level [73, 74].

Ripples in the linear amplitude and phase spectral responses of silicon photonic circuits are very common. There are many sources contributing to these ripples, including Fabry-Perot (FP) effects throughout the system, random waveguide roughness [75], and the imperfect control of input light polarization [76]. The FP effects are due to the reflections from the grating couplers (typically -20 dB optical return loss), fiber facets, Y-branch, etc. It is important to note that those issues are not fundamental and can be addressed with specific design techniques. For example, it is possible to reduce the FP effects by using grating couplers with low back reflection (-27 dB [77]), using fibers with AR-coated facets, and/or optimizing the Y-branch or replacing the Y-branch with alternative couplers. It is also possible to reduce the ripples with more dedicated polarization control. The waveguide roughness is challenging to control, but as the fabrication process improves, the roughness should be reduced in the future.

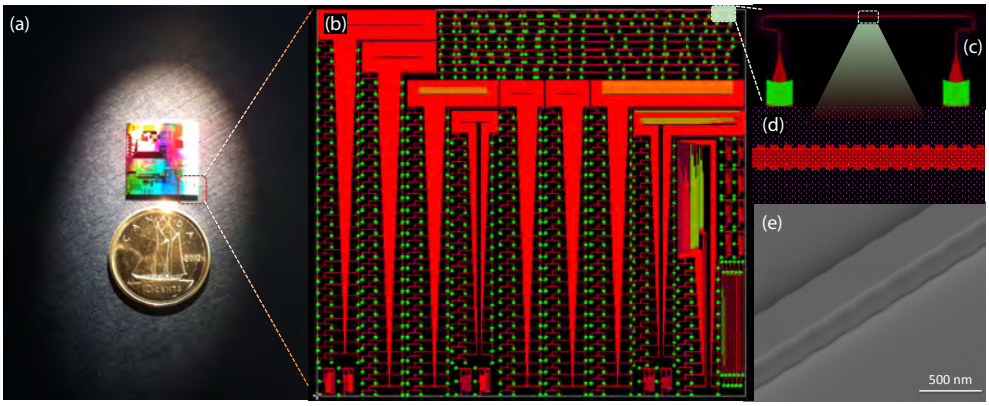


Fig. 1. Photo of the a SOI chip including a set of WBGs (a). Zoom of the WBGs mask layout (b). Single WBG (c, d). SEM image of the strip waveguide with sidewall corrugations (e)

In some cases, it is desirable to realize gratings with strong coupling (especially for broadband applications) and/or physically long. With the exception of resonators, in fact, long structures are generally needed to implement narrow bandwidth devices. Available fabrication techniques, however, often present limitations in the maximum size of the structures that can be reliably patterned in a stitching-free manner [78, 79]. It is generally very challenging to implement WBG with lengths exceeding a few millimeters. A possible solution to realize long integrated grating is to employ WGB in spiral waveguides [80]. However, an effective theoret-

#193416 - $15.00 USD Received 5 Jul 2013; revised 22 Sep 2013; accepted 27 Sep 2013; published 15 Oct 2013

ical model that could be used to design such WGBs is not yet fully available [68].

## 4. Integrated waveguide Bragg gratings for microwave photonics

Since the nineties, there has been an increasing interest on the possibility of realizing Bragg gratings on-chip to implement a variety of MWP functionalities in an integrated optical manner. To date, a relatively limited number of applications have been shown by the use of WBGs, covering applications that span from tunable delay generation to single-sideband (SSB) modulation. In our review, we will limit our attention to linear optical processors with application to MWP. We will neither cover works aiming at the realization of lasers, nor integrated chirped Bragg gratings for dispersion control, already treated e.g. in [84], as they are considered beyond the scope of a specific review on MWP signal processing and generation applications.

### *4.1. Tunable delays*

To our knowledge, the first proposal on the use of WBGs for MWP was presented in 1998 in a patent by Wickham [85] from TRW Inc. He showed a TTD design to be integrated on a planar silica waveguide with the aim of substantially reducing the package size of the device. The proposed device is composed by a polarization beam splitter, a polarization rotator and a spiral waveguide integrated on a single chip (Fig. 2(a)). The expected volume reduction when compared to a fiber implementation corresponds to a factor of about 35. Integrated Bragg gratings are placed at different distances along the spiral, to implement wavelength-selective reflectors providing several delay values that can be selected by changing the optical wavelength. The on-chip polarization beam splitter and the polarization rotator are used in conjunction in order to route the reflected waveform to a different port compared to the incident one, thus avoiding the use of a circulator. Alternatively, the same functionality can be implemented using a polarization sensitive Mach-Zehnder interferometer (PSMZI) and a quarter-wave polarization rotator (Fig. 2(b)).

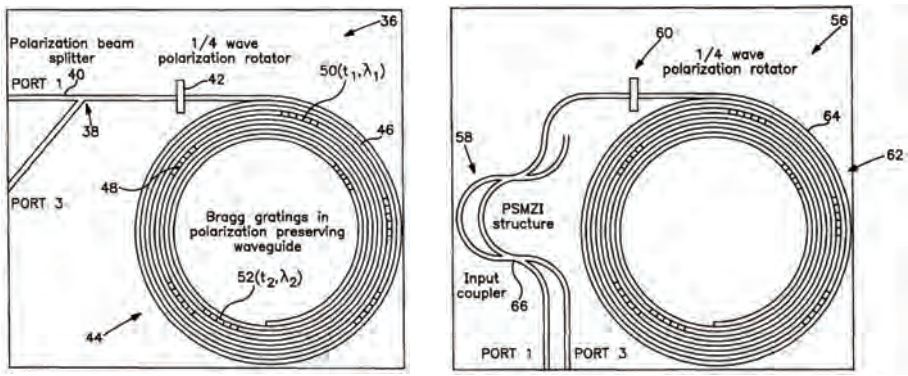


Fig. 2. Spiral waveguide with WBGs operated as a switched tunable delay line, with polarization beam splitter (a), and with PSMZI and quarter-wave polarization rotator (from [85])

More recently, Khan *et al.* [78] proposed analysis and theoretical design for the implementation of an integrated delay line that is low-loss, fast, compact, wavelength-independent and electronically-tunable. Three different device architectures are analyzed, based on apodized gratings, realized on silicon-on-insulator rib waveguides. In each grating the waveguide is straddled with a p-n junction diode. Upon application of a forward voltage to the p-n junction, the

#193416 - $15.00 USD Received 5 Jul 2013; revised 22 Sep 2013; accepted 27 Sep 2013; published 15 Oct 2013

refractive index of the waveguide can be changed, via free-carrier plasma effect. This methodology brings a two-fold advantage. First, the delay can be tuned without changing the optical wavelength; second, the use of electrical control allows a much faster delay tuning than using thermo-optical methods, which are limited to speeds in the order of milliseconds. For broadband operation (>20 Gb/s) the authors predict a maximum delay of approximately 40 ps with a loss of 10 dB. Lowering the speed requirement down to 1.6 Gb/s, the tuning range reaches 660 ps with a loss below 2.2 dB. This corresponds to a loss per time-delay unit of approximately 3.3 dB/ns, which is very low compared to state-of-the-art all-pass filters (APF, constituted by cascaded ORRs coupled to a common waveguide bus) [86, 87], coupled resonators optical waveguides (CROW, where resonators are side-coupled to each other) [57, 87, 88] or photonic-crystal (PhC) waveguides [78]. The expected device length is relatively high (approximately 2 cm) which is difficult to realize with e-beam techniques, thus eventually requiring the use of deep-ultraviolet optical lithography or nano-imprinting lithography.

Giuntoni *et al.* [79] showed the experimental demonstration of an integrated tunable delay line based on a a tapered integrated Bragg grating. Similarly to the work shown before, the delay tuning can be achieved without changing the optical wavelength, by use of a thermal tuning approach. The device is realized using deep-ultraviolet lithography and the structure features a constant etching depth of 50 nm, and a tapered rib waveguide width linearly increasing 150 $\mu$m over a 1-cm length (Fig. 3). Four gratings are arranged in a drop-filter configuration, which avoids the need of an optical circulator, and allows to double the total delay. A temperature variation of the whole chip between 32 and 38 degrees Celsius creates a variation of the total delay between approximately 0 to 440 ps, with a corresponding insertion loss varying between 1.7 and 6 dB. A full system performance analysis has been conducted, showing that the tunable delay line can operate up to 25 Gb/s. The performance in terms of maximum delay as well as optical loss per nanosecond (9.6 dB/ns) is comparable to the envisioned use of free-carrier plasma effect described previously.

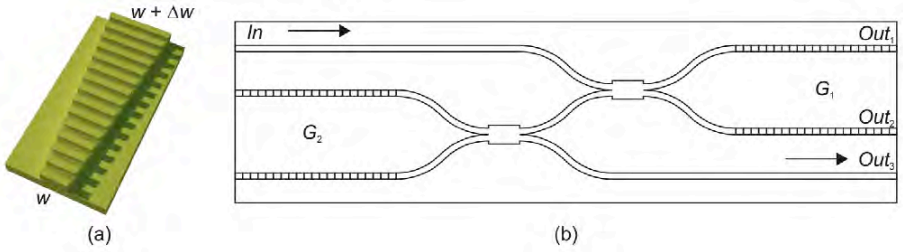


Fig. 3. Uniform Bragg grating on a tapered-width rib waveguide (a) and drop-filter configuration (b) (from [79])

More recently, Spasojevic and Chen [89, 90] demonstrated tunable delay lines using two different types of WBG architectures: side wall step chirped Bragg gratings and side wall serial grating arrays. In step chirped Bragg gratings, as the name suggests, a straight strip waveguide is employed where the grating is realized by corrugation along the sidewalls with a period changing discretely (in steps) along the grating length. Serial grating arrays, instead, consist of multiple distinct uniform gratings physically separated by straight waveguides, implementing a similar idea to the one proposed by Wickham [85]. Both approaches generate separate resonance bands, each characterized by a different delay amount, where the delay amount can be varied in steps by switching among different carrier wavelengths. The authors optimized their designs by transfer matrix solution of the coupled mode equations, and employed electron beam lithography for fabrication of their designed devices in silicon-on-insulator (SOI). 4 to

#193416 - $15.00 USD Received 5 Jul 2013; revised 22 Sep 2013; accepted 27 Sep 2013; published 15 Oct 2013

6 discrete delay steps have been implemented, which can be tuned by varying the wavelength across a range between 35 to 65 nm. The delay step varies between 15 to 25 ps and targets application to optical time division demultiplexing of optical communication signals with bitrate in the 40 Gbps range with 10 GHz bandwidth.

### *4.2. Optical differentiators*

Arbitrary-order optical integrators and differentiators have attracted considerable interest over recent years as they are fundamental building blocks to create a wide range of functionalities of interest for optical computing and signal processing, overcoming the intrinsic speed limitations of electronic solutions. They also find use in microwave applications, for example in ultra-wideband pulse re-shaping and processing [91, 92]. An optical differentiator of order $k$ computes the $k$-th time derivative of the complex-field envelope of an arbitrary optical waveform [93]. A number of schemes have been proposed, several of which are based on fiber grating devices [94–96]. The large benefit in terms of bandwidth that can be achieved via photonic integration can be seen in the implementation by Rutkowska *et al.* [81] of the first set of THz-bandwidth integrated photonic differentiators (Fig. 4). The devices are able to process ultrafast (sub-picosecond) optical pulses, and could also be applied for example to ultra-wideband pulse shaping. Each processor is realized using a Bragg grating in SOI with a very simple, $\pi$-phase shifted structure. The high coupling strength achievable with the integrated approach allows to implement a THz-bandwidth device while keeping the length at sub-millimeter scales, thus being orders of magnitude shorter and faster than differentiators based on their FBG counterparts [97].

### *4.3. Hilbert transformation and single sideband filtering*

Temporal Hilbert transformation (HT) is another important functionality in signal processing, with broad field of applications in telecommunications, radar, electronic countermeasures, computing and networking. Several optical implementations have been realized employing FBGs [99–101, 103]. Among others, HT can also be used to implement single sideband (SSB) modulation. Sima *et al.* [98, 104] demonstrated the first monolithically integrated all-optical SSB filter, realized in silica-on-silicon platform (Fig. 5). They employed a photonic Hilbert transformer (PHT), realized with a WBG with specific apodization profile and a single $\pi$-phase shift, following a similar design to that proposed by Asghari et al. [101], in conjunction with a spectral flat-top reflector. The flat-top reflector is realized using a sinc-apodized Bragg grating, having an amplitude spectrum ripple of only 1 dB and a bandwidth as wide as 200 GHz. The authors used a direct UV grating writing technique, which allows to realize arbitrary responses and does not require a phase mask. The gratings are connected to two parallel arms of an X-coupler. The distances between the coupler and the gratings are designed so that the reflected signals overlap with the correct phases in such a way that one of the two sidebands is cancelled out. A micro heater has been included in the design for accurate phase correction on the realized device, but in principle the fabrication accuracy should not require the use of any tunable structure. Suppression of the undesired sideband by $\sim$12 dB has been demonstrated at 6 GHz. The authors emphasize that the operative bandwidth is limited by the available measurement setup only, and that the PHT grating strength and the sideband suppression could be further increased by improving the phase trimming and the scattering methods employed. THz-bandwidth PHTs have been recently reported using improved WBG technology [102].

### *4.4. Microwave signal generation*

Bernhardi, Khan *et al.* [105, 106] have recently demonstrated the use of a monolithic dual-wavelength distributed-feedback (DFB) waveguide laser in ytterbium-doped aluminum oxide

#193416 - $15.00 USD Received 5 Jul 2013; revised 22 Sep 2013; accepted 27 Sep 2013; published 15 Oct 2013

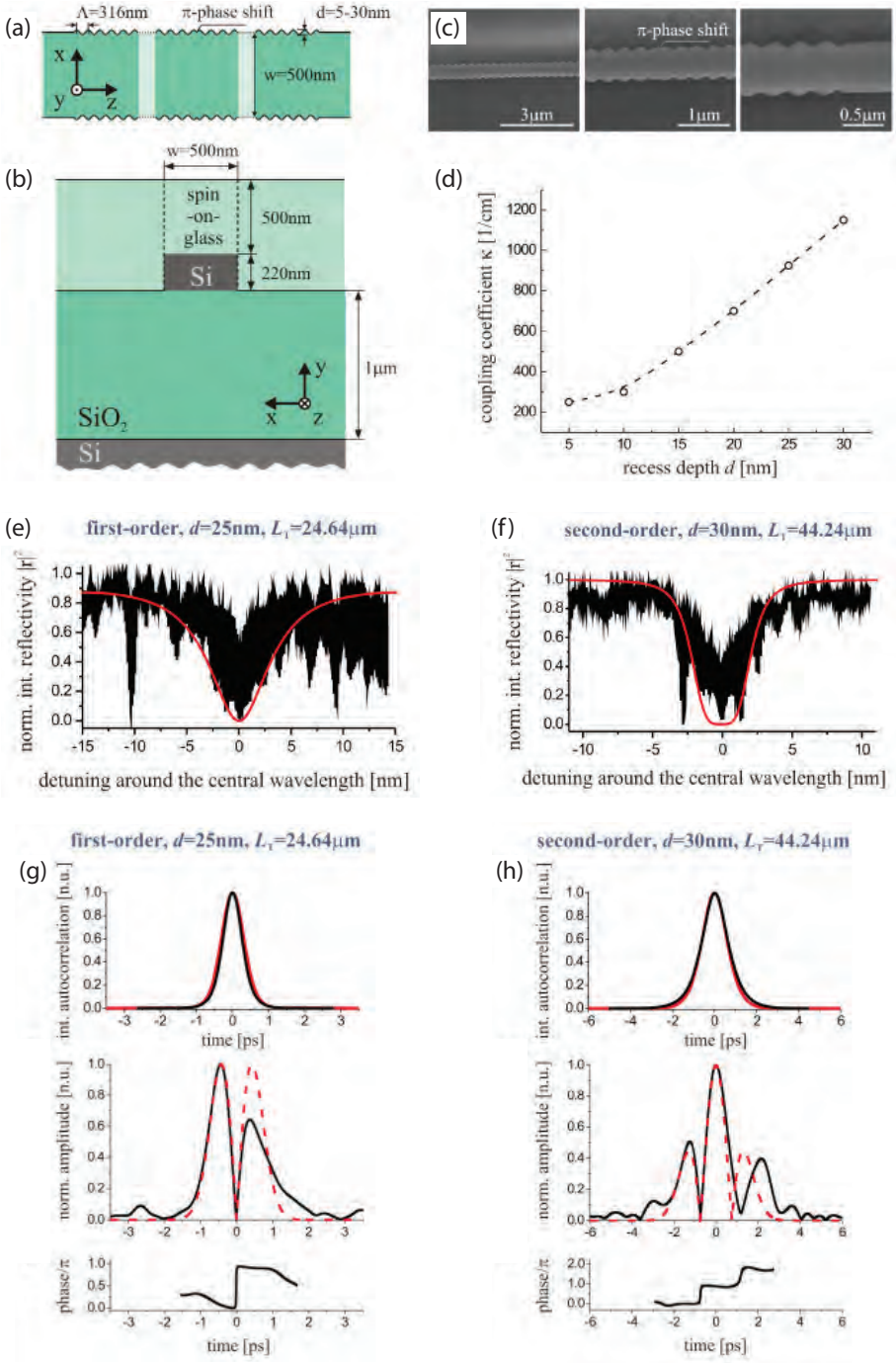


Fig. 4. Schematic (a), waveguide structure (b) and SEM images (c) of the temporal differentiator devices based on $\pi$-phase shifted WBG (in figure: $d$=30 nm). Coupling coefficient $\kappa$ versus recess depth $d$: this value also determines the operational bandwidth of the devices (d). Measured normalized intensity reflectivities for the first (e) and second order (f) differentiators compared to the theoretical responses. Time domain pulses before and after processing, for first (g) and second order differentiation (h) (from [98]).

#193416 - $15.00 USD Received 5 Jul 2013; revised 22 Sep 2013; accepted 27 Sep 2013; published 15 Oct 2013

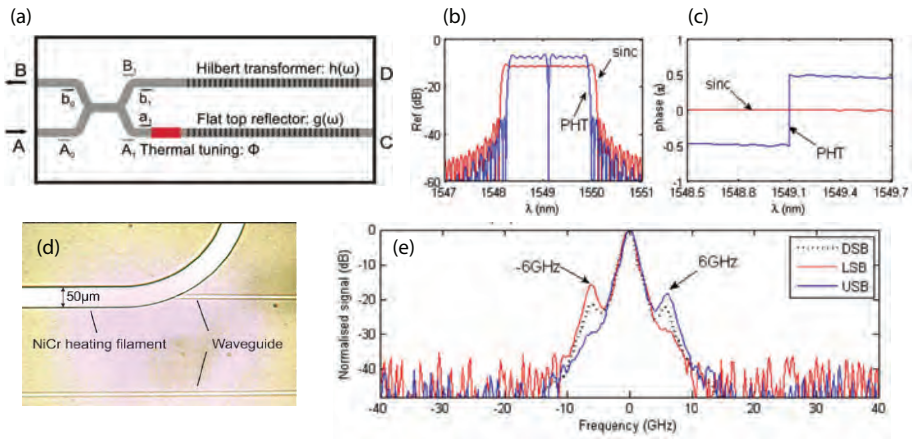


Fig. 5. Optial single-sideband filter architecture (a). Optical responses intensity (b) and phase (c) profiles of the PHT and of the broadband reflector. Picture of the heater tuning unit (c). Optical spectrum after SSB filtering (e) (from [98]).

for high-purity microwave signal generation. Radio frequency signal generation via optical means recently attracted large research interest, due to the fact that photonic generation allows to produce and distribute high frequency signals via low-cost optical fibers to large distances, with extremely low-loss when compared to electrical waveguides. The RF signal is generated by optical heterodyning, which consists in the generation of a beat signal between the two laser tones incoming on a photodetector at a frequency equal to the frequency spacing between the two optical frequencies.

The dual wavelength laser is realized using a 1-cm long Bragg grating, where two separated phase shifts are induced by creating two adiabatic sinusoidal widening of the waveguide width, long 2 mm each (Fig. 6(a)). They correspond to phase shifts values of $\pi/2+\pi/8$ and $\pi/2-\pi/8$. Those phase shifts induce two resonance peaks in the transmission band of the Bragg grating. Those peaks have the effect to induce two stable oscillations thus realizing a dual-wavelength laser with a single grating. The resonance wavelengths are equidistant from the Bragg wavelength and have the same amplitude and linewidth [107].

The proposed system is able to generate a microwave beat signal with 9 kHz linewidth at 15 GHz (Fig. 6(c)). The frequency deviation over a period of 45 minutes shows a standard deviation of approximately $\pm$2.5 MHz (Fig. 6(d)), and the power stability is within $\pm$0.35 dB.

Further experiments have shown a high degree of frequency stability and low phase noise for the generated microwave signal, which are crucial parameters in system applications. Khan *et al.* [106] implemented an optical frequency locked loop (OFLL) to stabilize a 14.21 GHz signal with a frequency stability of $\sim 1 \times 10^{10}$ over 1000 s time intervals, with a phase noise of 75 dBc/Hz at 1 MHz frequency offset.

## 5. A novel delay unit based on a simple dual PS-WBG

To illustrate further the unique potential of WBG for MWP signal processing applications, we report here a novel demonstration of a continuously tunable delay unit realized by means of a dual phase-shifted waveguide Bragg grating (DPS-WBG).

#193416 - $15.00 USD Received 5 Jul 2013; revised 22 Sep 2013; accepted 27 Sep 2013; published 15 Oct 2013

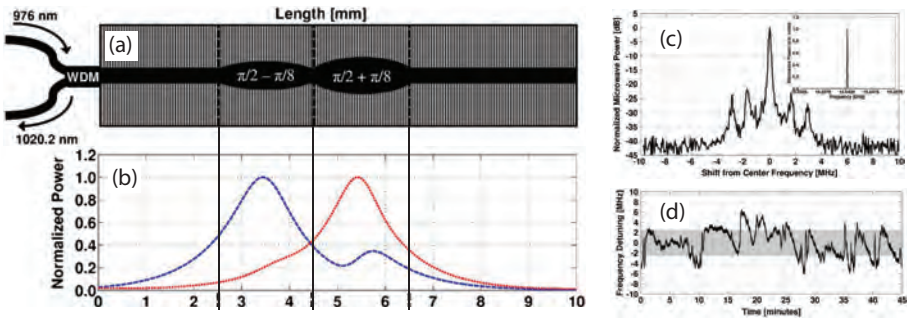


Fig. 6. Schematic of the dual-wavelength cavity based on Bragg grating (a), aligned with the calculated longitudinal field distribution of the respective laser wavelengths (b). Measured electrical spectrum (c) and RF frequency stability (d) (edited from [105]).

### *5.1. Motivation*

TTD units are fundamental processing units for a range of high-frequency, broadband RF signal processing applications; in particular they constitute basic building block for the implementation of beam forming networks for antenna arrays [108], ultra-wideband pulse shapers [92], and reconfigurable MPFs [1, 56, 109]. This work shows a continuously tunable delay up to 25.7 ps over a bandwidth of more than 8 GHz in a very compact unit measuring only 1.1 mm by 44 $\mu$m.

Several true-time-delay integrated photonic approaches have been proposed to date, the most common being optical resonators, photonic crystals, and apodized Bragg gratings [5, 56]. Nonetheless, for ORRs the RF bandwidth over which the ORR provide a constant delay is limited by the FSR; in addition, ORRs show a tradeoff between delay and bandwidths. Photonic crystals require fabrication accuracies in the order of tens of nanometers which make generally costly and low yield in the implementation. WBGs have been proposed, as seen in the previous literature review, to implement strongly dispersive devices where the tunability can be acheved by wavelength tuning. Nonetheless, the dispersion employed for delay tunability can become an issue when the unit is employed to delay broadband RF signals, which could experience a considerable delay variation across the RF band itself. Several researchers have analyzed the effects of this in-band delay variation (i.e. RF dispersion) in detail [71]. In this work, we propose a conceptually novel approach to the implementation of the TTD. We propose the use of a dual-phase shifted uniform and non-apodized Bragg grating on silicon. This results in an extremely simple layout which allows to relax the specifications in the fabrication process, mainly in terms of minimum feature size that can be reliably realized by the chosen process, not needing complex and accurate apodization profiles. The delay variation is still very flexible since it is based on tuning of the carrier frequency as in the case of dispersive gratings. Moreover, the measured response for a true-time delay line features an approximately all-pass intensity response. In comparison, ORRs show a higher attenuation for large delays [111]. In the approach reported here, the optical insertion loss in band is limited to 2.3 dB, with a ripple below 2.5 dB over the whole band (Fig. 7).

### *5.2. Optical response*

The optical reflection response of the DPS-WBG (Fig. 7) shows a steep phase shift around 194.5 THz which can be employed to generate a TTD on an RF signal, after optical single sideband modulation with full carrier (OSSB+C). The delay can be varied continuously by tuning the relative frequency positions between the modulated signal bandwidth and the phase shift, as will be described in the following.

#193416 - $15.00 USD Received 5 Jul 2013; revised 22 Sep 2013; accepted 27 Sep 2013; published 15 Oct 2013

An Optical Vector Analyzer (OVA) from Luna Technologies has been employed for the complete characterization (magnitude and phase response) of the PS-WBG. The reflection response in Fig. 7 shows a flat response with a ripple lower than 2.5 dB over the whole reflection band, with a notch of approximately 2.3 dB at 194.496 THz, that is, around the center of the reflection band. The measurement has been performed at a temperature of 21.1 degrees Celsius. The phase response shows a transition of approximately 300 degrees over 80 GHz, which can be used to implement the TTD functionality.

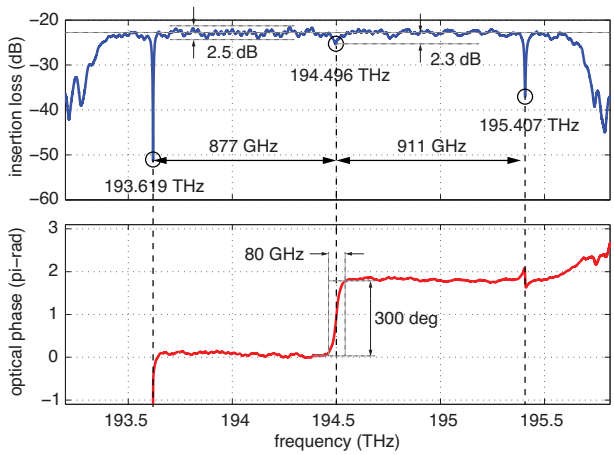


Fig. 7. Measured reflection intensity and phase spectrum of the DPS-WBG

The measured fiber-to-fiber insertion loss for the reflection response is approximately 23 dB, and includes the insertion loss of the external polarization controller, the grating couplers and the on-chip Y-branch [66]. This value can be reduced significantly by removing the polarization controller and using polarization maintaining fiber, and by optimizing the alignment stage and the quality of the fiber cleaving. It is important to note that the fundamental loss of the WBG is the waveguide propagation loss (mainly due to the sidewall roughness), which is in the range of 2-4 dB/cm. Assuming that the propagation loss is 3 dB/cm, the simulated insertion loss in reflection is very small, less than 0.01 dB. This is hardly measurable, as the calibration error could be $\pm 1$ dB or more.

### *5.3. Realization*

The DPS-WBG is realized using a 220 nm (thick) $\times$ 500 nm (wide) strip waveguide on SOI [110]. The sidewall corrugations depth is 100 nm and the grating period is 325 nm. Compared to the devices implementing similar functionalities presented in previously published works [78, 79, 90], the layout of this WBG is very simple, being realized by three uniform grating sections of 100, 200 and again 100 periods, separated by two phase shifts each 1 period-long (Fig. 8). Two separate phase shift sections are included in order to give sufficient degrees of freedom in the design stage to obtain an all-pass intensity response along the spectral region featuring the sharp phase shift (Fig. 7), which is crucial in the target TTD application. The total DPS-WBG length is about 130 $\mu$m. The use of a Y-junction on-chip allows to access the reflection port without the requirement for an off-chip circulator (Fig. 9). Input, transmission and reflection ports can be accessed via grating couplers (Fig. 9). The whole layout dimension is about 1.1 mm by 44 $\mu$m. The device was fabricated on a 200 mm SOI wafer at the IMEC foundry, with deep ultraviolet (UV) lithography and CMOS compatible fabrication equipment. A picture of the complete SOI chip is shown in Fig. 1.

#193416 - $15.00 USD Received 5 Jul 2013; revised 22 Sep 2013; accepted 27 Sep 2013; published 15 Oct 2013

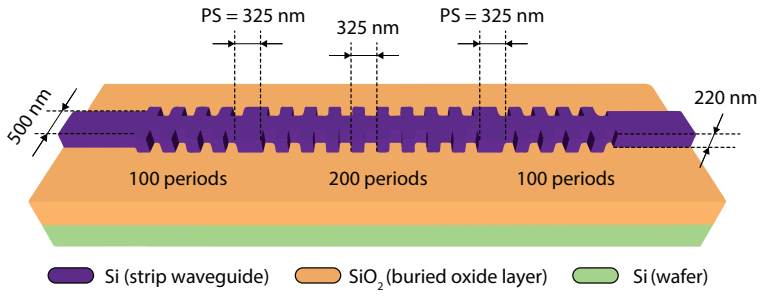


Fig. 8. Schematic of the PS-WBG used as TTD tunable delay

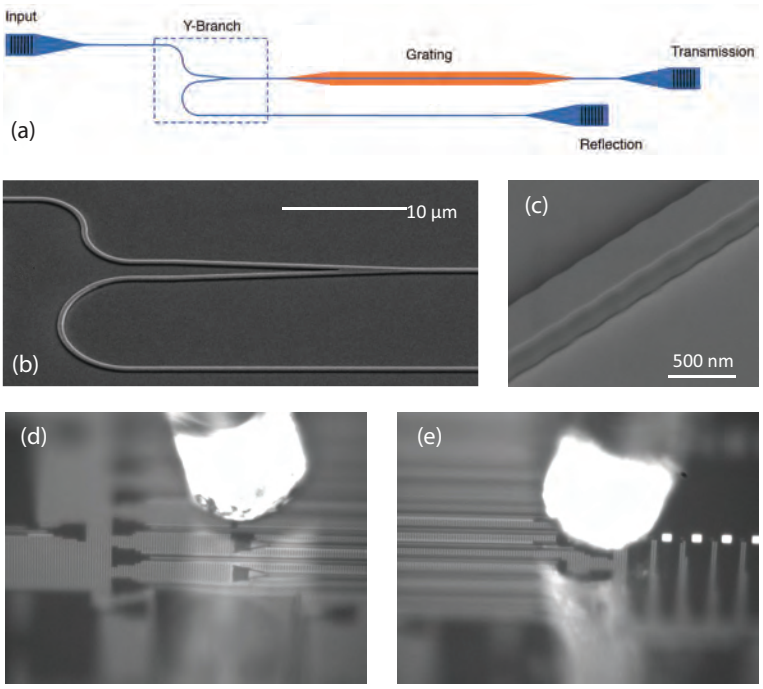


Fig. 9. Schematic of the waveguide layout (a), showing the Y-junction used to access the reflection port (b). SEM image of the rib waveguide with sidewall corrugations (c). Photo of the fiber coupling with the reflection (d) and input ports (e). (Images (a) and (b) edited from [66])

#193416 - $15.00 USD Received 5 Jul 2013; revised 22 Sep 2013; accepted 27 Sep 2013; published 15 Oct 2013

### 5.4. *Tunable true-time-delay generation*

In this subsection we show the principle of operation for use of the WBG device for TTD generation on broadband microwave signals.

An optical carrier at $\omega_c$ is intensity modulated (IM) by a passband RF signal with spectrum centered around $\omega_{RF}$. The modulated optical signal has a spectrum centered at $\omega_c + \omega_{RF}$. TTD operation requires the application of a constant group delay (thus a linear phase response) over the complete band of the modulated RF signal. The amount of group delay $\tau_g$ is determined by the slope of the linear phase spectral response $\varphi(\omega)$, at the frequency $\omega_c + \omega_{RF}$, according to the relation

$$\tau_g(\omega_c + \omega_{RF}) = \left. \frac{d\,\varphi(\omega)}{d\,\omega} \right|_{\omega = \omega_c + \omega_{RF}} \tag{1}$$

The proposed DPS-WBG can be employed to provide a tunable linear phase slope to an RF modulated signal. The phase transition around resonance shown in Fig. 7 can be employed to approximate a linear phase response around $\omega_c + \omega_{RF}$. Different phase slopes (corresponding to different constant group delays) can be obtained by simply changing the carrier frequency with respect to the resonance frequency (Fig. 10).

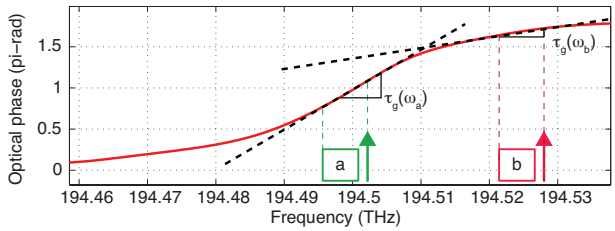


Fig. 10. Tunable TTD operation

Note that an all-pass intensity response is crucial in the target tunable delay application, where it is desirable that the RF magnitude response does not vary when tuning the group delay. Variations of intensity of the optical carrier and sideband while tuning the position of the optical carrier will directly translate to variations of the RF power output, which would need to be compensated for the targeted application, adding undesired complexity to the TTD system.

In the proposed device, the notch depth can be designed by adjusting the length mismatch between the two phase shift sections. This is demonstrated by the simulated responses shown in Fig. 11, showing that an increase in length mismatch translates into a reduction of the insertion loss in the notch. It is also important to note that the phase slope (thus the achievable maximum RF group delay) increases when the length mismatch increases, thus being ideally suited to implement delay lines with low insertion loss variation with respect to delay tuning.

Besides the width of the reflection band, the grating strength will also influence the maximum phase slope, thus the achievable RF delay (Fig. 12).

In this experiment, we propose the use of an OSSB+C modulation scheme. This allows to reduce the required delay bandwidth with respect to a double-sideband optical modulation scheme. In fact, it is sufficient to provide a linear phase over the optical bandwidth occupied by the carrier and one sideband only (Fig. 10). The use of full carrier modulation is proposed as this allows the use of a very simple direct detection scheme and avoids complex carrier re-insertion mechanisms [111]. RF measurements show generation of a continuously tunable TTD between 0 ps and 25.7 ps, on RF signals with a bandwidth up to approximately 8.5 GHz.

#193416 - $15.00 USD Received 5 Jul 2013; revised 22 Sep 2013; accepted 27 Sep 2013; published 15 Oct 2013

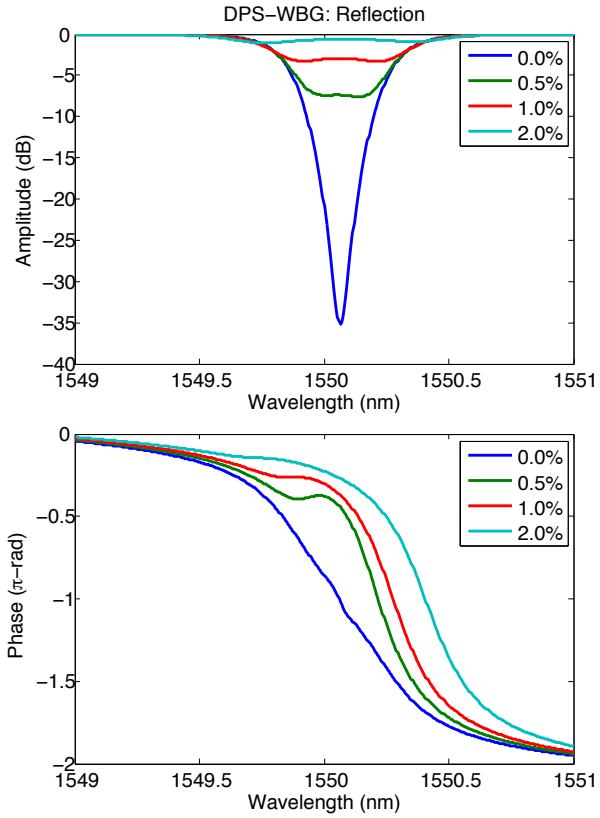


Fig. 11. Amplitude and phase responses of the DPS-WBG for different length mismatch between the phase shift sections

### *5.5. Experiment*

Fig. 13 shows the measurement setup for the RF characterization of the TTD line. A tunable continuous-wave (CW) laser with 10 mW optical power around 1550 nm provides the optical carrier. An Agilent 8722ES vector network analyzer (VNA) generates the RF signal to be processed. The desired OSSB+C modulation has been implemented using a dual parallel Mach-Zehnder modulator (DP-MZM), using the schematic described in [112]. The DP-MZM is fed by a 90-degrees hybrid from ET Industries Inc. The two 90-degrees out-of-phase RF outputs are connected with coaxial cables of the same length to the two RF inputs of the DP-MZM (Covega Mach-10 086), biased in a proper way to generate the target OSSB+C modulation. Fig. 14 shows the measured OSSB+C spectrum (RF input: 20 GHz, -5 dBm), where complete suppression of the undesired sideband is confirmed. The modulated signal enters a first erbium-doped fiber amplifier (EDFA), a polarization controller and then the optical chip in Fig. 6 for processing. Another EDFA is used to compensate for the fiber-to-chip coupling losses. A polarization controller is also placed before the DP-MZM to maximize the modulation efficiency. A Discovery Semiconductor DSC-R402PIN photodetector (PD, 3 dB bandwidth of 10 GHz, +4 dBm max. optical CW power) is used for direct detection of the processed signal, and connected to port 2 of the VNA for the RF phase measurements.

As discussed previously, a simple tuning of the optical carrier wavelength in the vicinity of the resonance of the DPS-WBG response allows continuous and seamless tunability of the RF

#193416 - $15.00 USD Received 5 Jul 2013; revised 22 Sep 2013; accepted 27 Sep 2013; published 15 Oct 2013

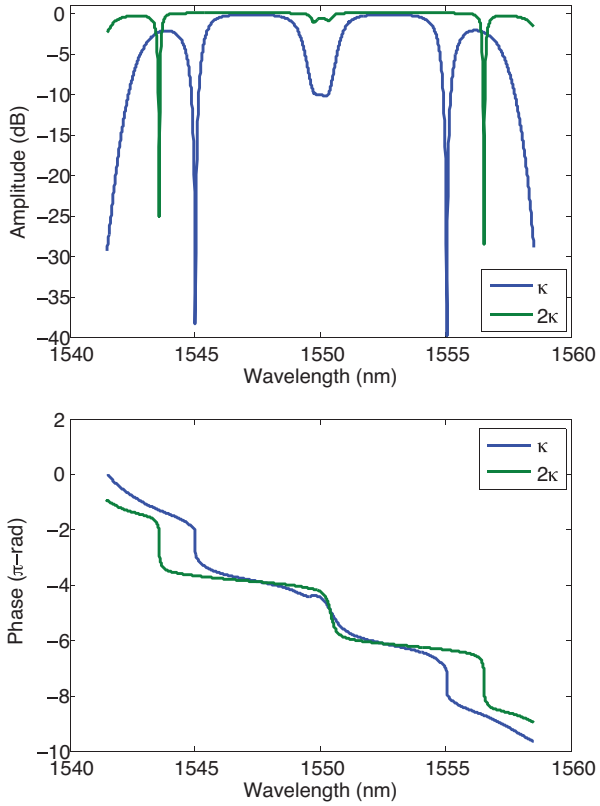


Fig. 12. Relative variation of amplitude and phase response (and in turn of the maximum RF delay) of the DPS-WBG for different grating strengths

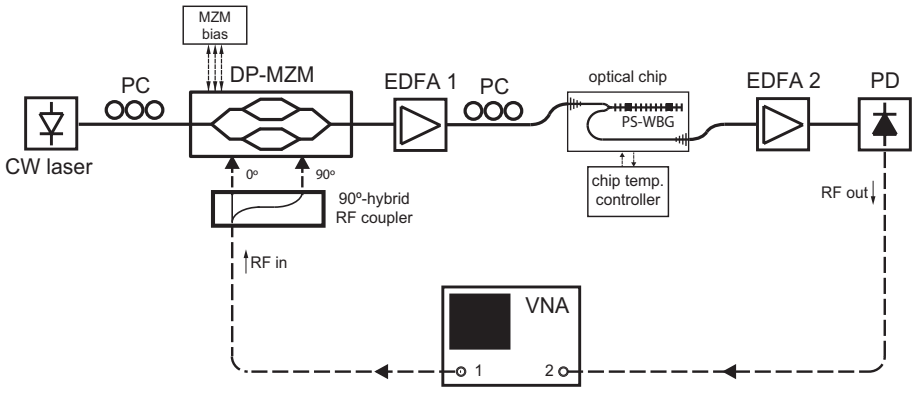


Fig. 13. Setup for continuously-tunable TTD demonstration

#193416 - $15.00 USD Received 5 Jul 2013; revised 22 Sep 2013; accepted 27 Sep 2013; published 15 Oct 2013

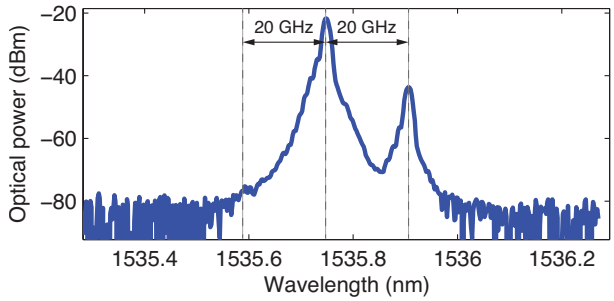


Fig. 14. Optical single-sideband spectrum. Resolution bandwidth of the optical spectrum analyzer set at the instrument minimum (0.01 nm) and high sensitivity settings.

group delay. Fig. 15 shows the achieved delay variation, between 0 ps to 25.7 ps, over an instantaneous RF bandwidth approximately between 1 to 8 GHz. Note that the maximum group delay achieved is in very good agreement with the maximum phase slope $\tau_g(\omega_a)$ obtained from the optical measurement shown in Fig. 10, which is approximately 9 deg / GHz, corresponding to a group delay of 25 ps. The shown phase responses have been obtained by subtracting from the measurements the one with minimum delay. The residual ripple visible in all the traces is attributed to the phase transfer function of the analog photonic link employed in the measurements. Nonetheless, the phase response in this frequency range can be considered sufficiently linear to provide constant group delay over the whole RF signal bandwidth.

The change in carrier wavelength required for tuning is minimal (0.39 nm), between 1535.94 nm (highest delay) and 1536.33 nm (lowest delay). A low-cost CW laser could be employed as the laser source in the system; thus, expensive lasers with wide tunability are not needed. The optical loss variation when tuning the delay value can be extracted from the measurements of the full (magnitude and phase) optical response shown in Fig. 7. The total delay-dependent variation of the insertion loss keeps within a range of 2.5 dB.

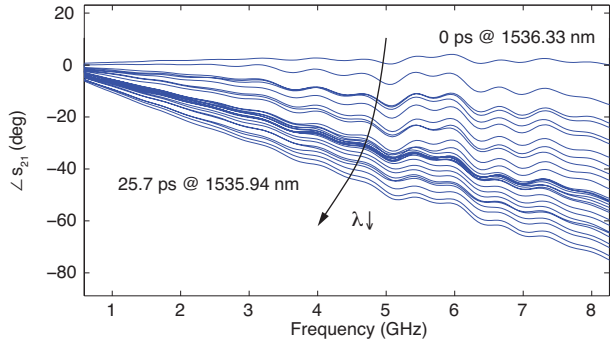


Fig. 15. RF phase response showing the seamless delay tunability

The required amount of delay is strongly application-dependent. For example, for application to phased array antennas, the higher the central frequency of the system, the smaller the antenna spacing and, in turn, the required delay needed to implement broadband beamsteering. As a practical example, let us consider the common case of a linear uniformly-spaced antenna array, operating at 8.5 GHz. The condition to avoid frequency squint for all steering angles, imposes that the antenna element spacing is half-wavelength (in air) or less, that is, 1.75 cm [108]. The

#193416 - $15.00 USD Received 5 Jul 2013; revised 22 Sep 2013; accepted 27 Sep 2013; published 15 Oct 2013

25 ps delay achieved in our case corresponds to approximately 7.5 mm of distance travelled by the RF wave in air. This amount of delay is sufficient to steer the antenna beam, without frequency squint, of approximately 26 degrees compared to broadside, comparable to many previous demonstrations of squint-free optically controlled antennas using integrated ORRs [113, 114], but with a strong reduction of the length of the delay unit (130 $\mu$m versus few centimeters for ORRs in silicon nitride technology [115]).

### *5.6. Example of application*

To demonstrate the negligible effect of the phase ripples, we analyze their effect on the example application described above, i.e. an optically-controlled phased array antenna (8 element linear array operating up to 8.5 GHz). Fig. 16 shows the simulated antenna directivity pattern versus frequency that would be obtained when the proposed delay line were used as basic delay unit. In this test we have included the measured responses of Fig. 15 in the simulation of the radiation patterns. It is possible to observe that the main lobe, indicated by the dotted line in the middle of the brightest area, keeps in the desired pointing direction with an error always below $\pm 2^\circ$ (the maximum of radiation varies from $24.7^\circ$ to $28.6^\circ$). Considering that the 3-dB bandwidth of the radiation beam in its narrowest point at 8.5 GHz is $14.05^\circ$ the maximum of radiation is always within the main lobe of radiation at all frequencies. This result proves that the effect of the phase variation is hardly noticeable from the system point of view, keeping squint-free operation over a bandwidth from below 1 GHz to above 8.5 GHz. At the same time, we have shown that a noticeable beamsteering (approx. 26 degrees) can already be achieved with the a delay amount of 25.7 ps.

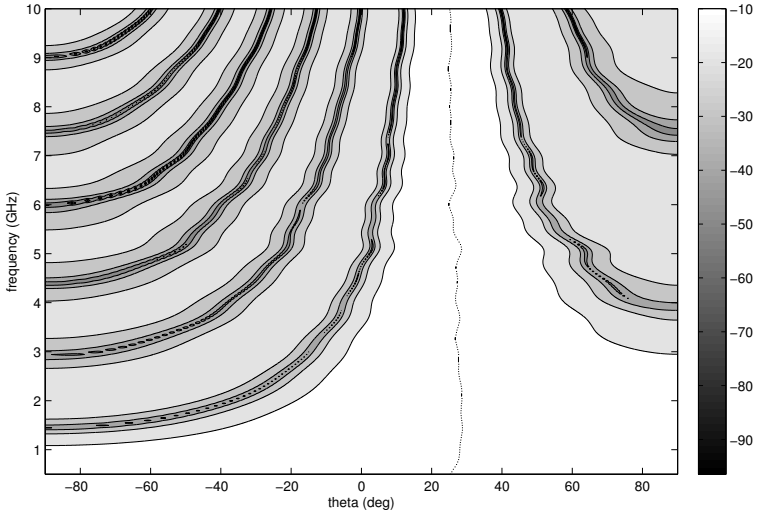


Fig. 16. Simulated directivity pattern of an 8-element uniform and equally-spaced (1.75 cm) phased array antenna optically-fed using the proposed DPS-WBG as basic delay unit. Note the squint-free behaviour over the complete band of operation.

### *5.7. Temperature tuning*

An alternative way to realize delay tuning is to modify the temperature of the chip. Employing a very simple and low-cost temperature feedback control system based on a Peltier element

#193416 - $15.00 USD Received 5 Jul 2013; revised 22 Sep 2013; accepted 27 Sep 2013; published 15 Oct 2013

actuator and a temperature-sensitive resistor, an accurate and stable tuning of the position of the optical resonance with temperature has been achieved. Fig. 17 shows a photo of the employed temperature control setup, where the chip (a) is mounted on a copper plate (b), connected to a heat sink (c) via a Peltier element (d). A temperature sensitive resistor is inserted in the brass plate (e) and uses thermal conductive paste to minimize the thermal resistance. A commercial temperature controller with 0.1 K accuracy has been employed.

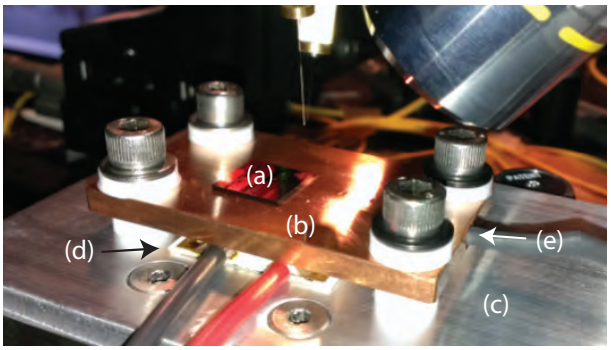


Fig. 17. Temperature control setup

Tuning ranges in excess of 500 GHz can be easily reached with a temperature change between 1 °C and 55 °C, with a rate of approximately 9.44 GHz/°C (Fig. 18) [116]. Besides being used for tuning the delay, the temperature change can be advantageously employed for calibration of the processor, for example to allow its operation around the CW wavelength range of interest. This can be useful for example when employing a low-cost CW laser with limited tunability.

Thanks to the employed temperature control technique, using heat conductive paste and a bulk copper block with active temperature feedback at chip scale, temperature variations across the total grating length ($\approx 130\mu$m) are expected to be very small and therefore to have very little effect on the WBG response; however, they could be more significant at chip-scale or wafer-scale. When multiple devices are employed to implement a more complex signal processor, separate temperature actuators (heaters) localized in correspondence of each device could be used to implement a more accurate control of the temperature across the chip. A similar approach has been successfully employed in previous works [5, 57].

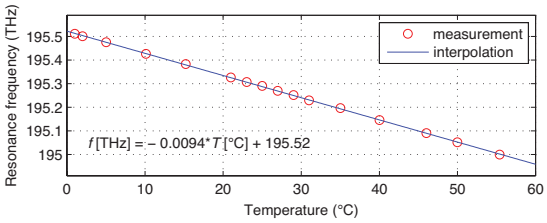


Fig. 18. Variation with temperature of the central frequency of the phase shift of the PS-WBG

Note that the simple layout of the DPS-WBG can be modified to create larger phase shifts while keeping the same all-pass configuration. This can be done by inserting additional, properly engineered phase shift sections, in order to increase the amount of delay and/or the usable delay bandwidth, thus creating a very flexible delay unit.

#193416 - $15.00 USD Received 5 Jul 2013; revised 22 Sep 2013; accepted 27 Sep 2013; published 15 Oct 2013

In Table 1 we show a summary of the above-described MWP applications to date that make use integrated WBGs, including the TTD work reported here for the first time.

Table 1. Reported results of integrated WBGs for MWP applications (* indicates theoretical work)

| Year | Functionality | WBG type | Material | 1st author [Ref.] | Figure of merit |
|---|---|---|---|---|---|
| 1998 | delay | not specified | not specifed* | Wickham [85] | not specified |
| 2011 | delay | apodized-WBG (rib) | SOI* | Khan [78] | delay = 40 ps; BW $>$ 20 Gb/s |
| 2011 | differentiator | PS-WBG (ridge) | SOI | Rutkowska [81] | BW $>$ 1 THz |
| 2012 | LO generation | DFB (laser), 2 PS | $Al_2O_3$:$Yb^{3+}$ | Bernhardi, Khan [105, 106] | $\pm$2.5 MHz, $\pm$0.35 dB |
| 2012 | delay | tapered (rib) | SOI | Giuntoni [79] | delay = 440 ps; BW = 25 Gb/s |
| 2013 | SSB modulator | apod. PS + sinc-apod. | silica-on-Si | Sima [98, 104] | $\sim$12 dB suppression |
| 2013 | delay | step-chirped grating | SOI | Spasojevic [89] | delay $\sim$125 ps; BW = 10 GHz |
| 2013 | delay | phase-shifted WBG | SOI | Burla [this work] | delay = 25.7 ps; BW $>$ 8 GHz |

## 6. Contra-directional couplers (CDCs)

In our demonstration of Section 5 we have shown how an on-chip Y-branch has been employed in order to access the reflection port of a WBG device. This structure removes the need for an off-chip circulator, but inherently adds a minimum of 6 dB of optical loss in the signal path. This loss translates in an RF loss of 12 dB for the MWP signal processor, due to the quadratic relation between optical loss and RF gain in an MWP link [5]. Recently, Shi *et al.* [117, 118] implemented a 4-port optical device, known as contra-directional coupler (CDC), on the SOI platform. This type of device was first introduced by Tan *et al.* in [119]. A CDC is an add-drop filter whose transfer function is defined by a Bragg grating. The insertion loss of a CDC is ideally 0 dB, and it can thus be advantageously employed in virtually all applications requiring a Bragg grating in conjunction with an optical circulator. In fact, it enables the integration of Bragg-grating-defined functions on-chip, without using a circulator [118]. If employed in the schematic of Fig. 9(a), it could replace the Y-branch and the WBG in reflection, thus allowing an RF insertion loss improvement as high as 12 dB.

In addition to that, compared to filters using RRs, CDC can provide wider channel bandwidths, since they do not operate in multiple simultaneous longitudinal modes as for the RRs, thus the bandwidth is not limited by the free spectral range [120]. The schematic of a CDC and image of the realized device are shown in Fig. 19. In [118], the CDC was also shown to be electrically tunable using free-carrier injection.

To achieve even broader usable bandwidths, a novel design was proposed very recently [120] to remove the internal back-reflections which limit the usable spectral bandwidth of CDCs. This novel architecture employs out-of-phase gratings and is known as anti-reflective contra-directional coupler (AR-CDC). With this technique, single-band operation up to 180 nm with a

#193416 - $15.00 USD Received 5 Jul 2013; revised 22 Sep 2013; accepted 27 Sep 2013; published 15 Oct 2013

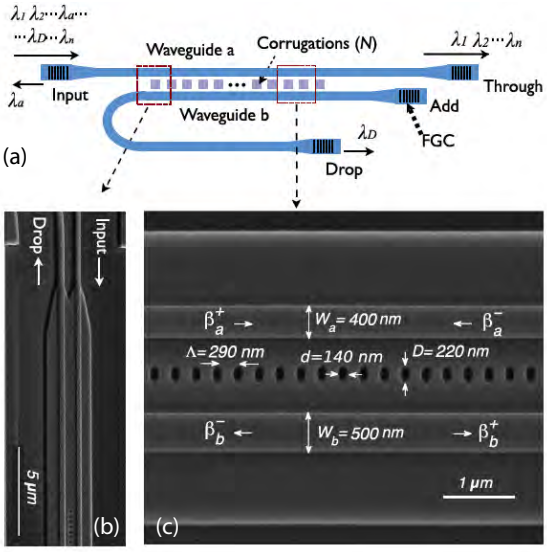


Fig. 19. (a) schematic layout of the proposed CDC. (b) SEM image of the tapers (c) SEM image of the device corrugations (edited from [117]).

single, flat-top passband as wide as 13 nm has been demonstrated.

## 7. Integrated WBGs in silicon photonics for MWP applications

### *7.1. WBGs as basic building blocks for signal processing*

Very attractive possibilities come from the use of silicon photonics to implement WBGs for MWP applications. We believe that WBGs should provide their full signal processing potential when employed as signal processing/shaping units to implement highly-complex MWP processors (e.g. multitap fully-programmable MPFs [1], complex reconfigurable beamforming networks [5], flexible arbitrary waveform generators [121], and more). Particularly attractive will be the use of Bragg gratings in CDC configuration, which, as described in Section 6, allows to minimize the insertion loss and, in turn, the possibility to cascade multiple units to implement complex functionalities without sensibly decreasing the link gain, which is paramount in MWP applications [70]. Also, CDCs have already proven to be electrically tunable [118] and, in anti-reflective configuration they showed very broadband performance over bandwidths in the order of hundreds of nanometers [120].

We have discussed how the high cost and low reliability of current MWP solutions originates from the need of using discrete components, such as modulators, photonic processors and photodetectors, which need separate packaging and individual interconnections to optical fibers [5]. The perspective of integrating multiple active and passive functions on a single chip allows to reduce significantly the cost of the resulting devices while improving system stability and reliability. Additionally, this should enable the implementation of entirely novel functionalities (e.g. optical phase fluctuations due to temperature and mechanical stress can be eliminated by removing optical fibers, and consequently, coherent signal processors become also possible). The demonstrated capability to implement active functionalities on silicon [63] and to integrate silicon with active III/V devices and lasers [59, 62] opens an attractive perspective on the MWP scenario. We believe it would be very attractive to exploit these proven hybrid

#193416 - $15.00 USD Received 5 Jul 2013; revised 22 Sep 2013; accepted 27 Sep 2013; published 15 Oct 2013

integration possibilities to build full systems where fiber-to-chip coupling, signal transport and delay are done in silicon nitride ultra-low-loss waveguides, processing is performed in compact silicon photonics WBGs and active functions can be realized either directly in silicon or in hybrid integration of III/V materials, as described in Sec. 3.1. In particular, a unified model for the analysis of MWP systems was recently presented, based on the concept of a filtered MWP link [122]. Besides its use as a practical analysis tool, this model suggests the possibility to realize a general-purpose reconfigurable MWP signal processor, which could implement many different MWP functions [123], and could in principle be integrated on a single photonic chip (Fig. 20).

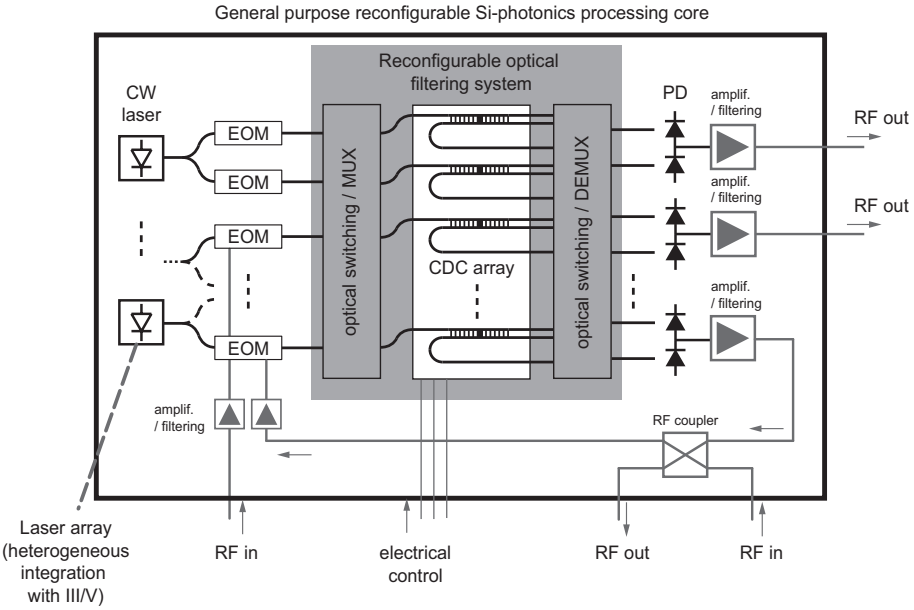


Fig. 20. Envisioned schematic of a general purpose reconfigurable MWP signal processor based on CDCs. EOM: electro-optic modulator; PD: photodetector.

The unique possibility offered by silicon photonics to realize highly-complex reconfigurable photonic processors on-chip with high yield could allow the realization of such a general purpose MWP processor. The reconfigurable filtering could be provided by WBGs in a CDC configuration, possibly in conjunction with other signal processing devices, and the active functionalities could be realized directly in silicon or via heterogeneous integration with III/V materials. In a somehow longer term, such an all-purpose, integrated programmable processor could be produced in a large scale leveraging the already existing CMOS facilities. This would enable significantly reducing the unit cost while improving the key performance specifications of MWP processors, thus representing a very attractive prospect towards their commercial success.

## 8. Conclusion

In this paper we have reviewed recent advances on implementations of MWP functionalities using WBGs, with particular emphasis to the performance improvements offered by the integrated realization of these devices. We expect that many of the microwave signal processing functionalities previously demonstrated with FBGs can be directly transferred into integrated optical formats by harnessing the potential of WBGs as versatile and reconfigurable signal processing

#193416 - $15.00 USD Received 5 Jul 2013; revised 22 Sep 2013; accepted 27 Sep 2013; published 15 Oct 2013

engines. This will allow to retain the unique design versatility of FBG-based linear optical filters, plus adding the attractive advantages given by an integrated realization. In line with this, we have reported here the experimental demonstration of a novel, compact and fully tunable TTD line based on a very simple PS-WBG implemented in SOI technology. We believe that the proven design flexibility of WBGs, in conjunction with the unique strength of silicon photonics to enable system-level integration of reproducible high-performance devices, will open the path towards the implementation of highly-complex MWP processors with an improved performance, and potentially much higher yield and lower cost than other competing technologies, as needed for the spread of MWP solutions into real-world, commercial applications.

**Acknowledgements**

The authors would like to acknowledge CMC Microsystems for enabling the fabrication of the silicon chips via ePIXfab, Lumerical Solutions Inc. and Mentor Graphics for the design software, and funding from the Natural Science and Engineering Research Council of Canada (NSERC), in particular from the Canada Research Chair and SiEPIC CREATE programs. M. Burla, L. Romero Cortés and J. Azaña would like to thank Prof. T. Denidni and Dr. A. Gijo for their assistance with the RF measurement equipment. M. Burla would also like to thank Dr. David Marpaung for the fruitful discussions.

#193416 - $15.00 USD Received 5 Jul 2013; revised 22 Sep 2013; accepted 27 Sep 2013; published 15 Oct 2013